

University of Alberta

A Study of Horizontal Stratified Flow in a Duct

by

Patricia Pernica



A thesis submitted to the Faculty of Graduate Studies and Research in  
partial fulfillment of the requirements for the degree of Master of Science.

Department of Mechanical Engineering

Edmonton, Alberta  
Fall 2007



Library and  
Archives Canada

Bibliothèque et  
Archives Canada

Published Heritage  
Branch

Direction du  
Patrimoine de l'édition

395 Wellington Street  
Ottawa ON K1A 0N4  
Canada

395, rue Wellington  
Ottawa ON K1A 0N4  
Canada

*Your file* *Votre référence*  
*ISBN: 978-0-494-33326-6*  
*Our file* *Notre référence*  
*ISBN: 978-0-494-33326-6*

#### NOTICE:

The author has granted a non-exclusive license allowing Library and Archives Canada to reproduce, publish, archive, preserve, conserve, communicate to the public by telecommunication or on the Internet, loan, distribute and sell theses worldwide, for commercial or non-commercial purposes, in microform, paper, electronic and/or any other formats.

The author retains copyright ownership and moral rights in this thesis. Neither the thesis nor substantial extracts from it may be printed or otherwise reproduced without the author's permission.

#### AVIS:

L'auteur a accordé une licence non exclusive permettant à la Bibliothèque et Archives Canada de reproduire, publier, archiver, sauvegarder, conserver, transmettre au public par télécommunication ou par l'Internet, prêter, distribuer et vendre des thèses partout dans le monde, à des fins commerciales ou autres, sur support microforme, papier, électronique et/ou autres formats.

L'auteur conserve la propriété du droit d'auteur et des droits moraux qui protègent cette thèse. Ni la thèse ni des extraits substantiels de celle-ci ne doivent être imprimés ou autrement reproduits sans son autorisation.

---

In compliance with the Canadian Privacy Act some supporting forms may have been removed from this thesis.

Conformément à la loi canadienne sur la protection de la vie privée, quelques formulaires secondaires ont été enlevés de cette thèse.

While these forms may be included in the document page count, their removal does not represent any loss of content from the thesis.

Bien que ces formulaires aient inclus dans la pagination, il n'y aura aucun contenu manquant.

  
**Canada**

## ABSTRACT

An investigation was carried out on horizontal wavy stratified flow in a rectangular duct in order to fulfill two objectives. The first objective was to characterize the gas-liquid interface. This was done through the development of a non-contact film thickness measurement technique that utilized laser induced fluorescence and high speed videography. The second objective was to determine the effects of various concentrations of a drag reducing additive (DRA) on the horizontal stratified wavy two phase flow. Wave characteristics, average film heights, RMS wave heights, frequency analysis and pressure drop measurements with and without DRA were explored. The data gathered from the developed measurement technique yielded similar results to previous comparable studies. The results from the addition of DRA demonstrated a significant change in almost all parameters discussed, with the addition of only 10 ppm DRA. Maximum change in parameters occurred for concentrations of DRA between 30ppm and 40 ppm. Comparisons between pressure drop and interfacial friction factor suggested that the addition of DRA had a large effect on the gas-liquid interface.

## ACKNOWLEDGEMENTS

There are numerous people without whom all of this would not have been possible. I would like to thank my two supervisors, Dr. Brian Fleck and Dr. Ted Heidrick for their support throughout this project. Their guidance and expertise were critical to my success.

I would also like to thank past and present students in the lab group: Wayne Klaczek for all his help in designing the experimental apparatus, Luis Torres and Marc Huot for their tireless help setting up equipment and Doug Langer for his willingness to answer my numerous questions. Special thanks to the machinists, technicians and office staff in the Department of Mechanical Engineering especially Dirk Kelm, Bernie Faulkner, Greg Miller and Terry Nord.

Finally I wish to thank my family and friends whose support and encouragement helped me through all the tough times, especially Graeme Watson whose unwavering encouragement and advice were essential to the completion of this thesis.

Financial support from the Faculty of Graduate Studies, Department of Mechanical Engineering and the Graduate Students' Association is also gratefully acknowledged.

# CONTENTS

<b>1</b>	<b>Introduction</b>	<b>1</b>
1.1	Introduction . . . . .	1
1.1.1	Motivation . . . . .	2
1.2	Background . . . . .	4
1.2.1	Stratified Flow . . . . .	4
1.2.2	Influence of Waves in Stratified Flow . . . . .	8
1.3	Research Objectives . . . . .	13
1.4	Thesis Outline . . . . .	13
<b>2</b>	<b>Measurements of Wavy Stratified Flow</b>	<b>18</b>
2.1	Introduction . . . . .	18
2.2	Background . . . . .	19
2.2.1	Previous Research Work in Stratified Flow . . . . .	19
2.2.2	Film Thickness Measurement Techniques . . . . .	22
2.3	Apparatus . . . . .	24
2.3.1	Experimental Apparatus . . . . .	24
2.3.2	Orifice Meter Calibration and Flow Verification . . . . .	29
2.3.3	Rotameter Calibration . . . . .	31
2.3.4	Laser Set-up . . . . .	31
2.3.5	Camera Set-up . . . . .	32
2.4	Measurement Method . . . . .	33
2.4.1	Pressure and Flow Rate Measurements . . . . .	35
2.4.2	Interface Measurements . . . . .	35
2.4.3	Repeatability . . . . .	40
2.4.4	Systems and Test Conditions . . . . .	41
2.5	Results and Discussion . . . . .	42
2.5.1	Interfacial Waves . . . . .	42
2.5.2	RMS Wave Heights . . . . .	49

2.5.3	Pressure Drop . . . . .	51
2.5.4	Wave Frequency . . . . .	57
2.6	Conclusion . . . . .	61
<b>3</b>	<b>Drag Reduction</b>	<b>66</b>
3.1	Introduction . . . . .	66
3.2	Background . . . . .	67
3.3	Experimental Setup and Method . . . . .	71
3.4	Experimental Results . . . . .	74
3.4.1	Introduction . . . . .	74
3.4.2	Effect of DRA on Interfacial Waves and Flow Regime . . . . .	74
3.4.3	Effect on Average Film Thickness . . . . .	76
3.4.4	RMS Wave Heights . . . . .	78
3.4.5	Drag Reduction . . . . .	84
3.5	Conclusion . . . . .	95
<b>4</b>	<b>Conclusion</b>	<b>102</b>
<b>A</b>	<b>Orifice Plate</b>	<b>105</b>
<b>B</b>	<b>Digital Filter</b>	<b>108</b>

## LIST OF TABLES

2.1	Interface data collected at $U_{GS}=16$ m/s and $U_{LS}=0.06$ m/s over 2 seconds, 5 seconds and 8.7 seconds . . . . .	40
2.2	Summary of the repeatability tests. The average heights and RMS wave height results are for the centre of the duct. . . . .	41
2.3	A summary of the interface data collected with the laser-camera setup. . . . .	45
3.1	A summary of the $f_i/f_s$ results for all flow conditions . . . . .	92

## LIST OF FIGURES

1.1	Schematic of Stratified Flow . . . . .	5
1.2	Front View of Stratified Flow . . . . .	7
1.3	Sub-Regimes of Stratified Flow . . . . .	10
2.1	Experimental Apparatus . . . . .	25
2.2	Apparatus Screw-Slot System . . . . .	26
2.3	Water Inlet of the Apparatus . . . . .	27
2.4	Orifice Plate . . . . .	30
2.5	Laser Setup . . . . .	33
2.6	Camera Setup . . . . .	34
2.7	Repeatability Laser Mark . . . . .	34
2.8	Laser Light Reflection . . . . .	36
2.9	Image Processing Procedure . . . . .	38
2.10	Surface Film Thickness Plot . . . . .	43
2.11	Low Pass Filter Results . . . . .	44
2.12	Instantaneous Film Height for $U_{GS} = 12m/s$ and $U_{LS} = 0.04m/s$	47
2.13	Instantaneous Film Height for $U_{GS} = 14m/s$ and $U_{LS} = 0.04m/s$	48
2.14	Dimensionless Average Film Height . . . . .	48
2.15	RMS Film Heights . . . . .	50
2.16	Definition of $\Delta h$ . . . . .	50
2.17	Mean Large Wave Amplitude as a Function of RMS Wave Heights . . . . .	51
2.18	Pressure Drop . . . . .	52
2.19	Interfacial Friction Factor . . . . .	55
2.20	Rectangular and Circular Cross-Section Geometries . . . . .	56
2.21	Power Spectral Density . . . . .	57
2.22	Dominant Wave Frequency . . . . .	59
2.23	Power Spectral Density as a Function of $U_{GS}$ . . . . .	60

3.1	Comparison of Instantaneous Dimensionless Film Height . . . .	75
3.2	Comparison of Waves for Various Concentrations of DRA . . . .	77
3.3	Comparison of Average Dimensionless Film Heights for Various Concentrations of DRA . . . . .	79
3.4	Comparison of Average Dimensionless Film Heights with Concentrations of DRA that Produced Maximum Drag Reduction	80
3.5	Effect of DRA on $h_{RMS}$ . . . . .	81
3.6	Relationship Between $h_{RMS}$ and $U_{LS}$ . . . . .	82
3.7	Relationship Between $dH$ and Concentration of DRA . . . . .	83
3.8	Large Wave Amplitude as a Function of RMS Values of Film Thickness . . . . .	84
3.9	Pressure Drop for Various Concentrations of DRA . . . . .	85
3.10	Drag Reduction as a Function of $U_{GS}$ . . . . .	86
3.11	Drag Reduction as a Function of DRA concentration . . . . .	88
3.12	Friction Factor as a Function of Concentration of DRA . . . . .	94
3.13	Friction Factor as a Function of $U_{GS}$ . . . . .	94
3.14	Friction Factor as a Function of $U_{LS}$ . . . . .	95
B.1	Digital Filter . . . . .	109

## NOMENCLATURE

$A$	.....	cross-sectional area
$D_h$	.....	hydraulic diameter
$\frac{dp}{dx}$	.....	pressure drop
$DR$	.....	Drag Reduction
$f$	.....	friction factor
$h$	.....	instantaneous film thickness
$\bar{h}$	.....	average film thickness
$h_{RMS}$	.....	RMS wave height
$k_m$	.....	wave number
$\dot{m}$	.....	mass flow rate
$P$	.....	perimeter
$Q$	.....	volume flow rate
$Re$	.....	Reynolds number
$S$	.....	interface length
$U$	.....	velocity
$X$	.....	Lockhart-Martinelli parameter

Greek symbols:

$\bar{\alpha}$	.....	liquid hold-up
$\beta$	.....	ratio of inner to outer orifice diameter
$\theta$	.....	dimensionless viscosity
$\mu$	.....	dynamic viscosity
$\nu$	.....	kinematic viscosity
$\rho$	.....	density
$\sigma$	.....	surface tension
$\tau$	.....	shear stress
$\phi$	.....	Lockhart-Martinelli multiplying factor

subscripts:

$G$	.....	gas phase
$GS$	.....	superficial gas phase
$i$	.....	gas-liquid interface
$L$	.....	liquid phase
$LS$	.....	superficial liquid phase
$s$	.....	single phase

# CHAPTER 1

## INTRODUCTION

### 1.1 Introduction

Understanding stratified flow including smooth stratified, wavy stratified and stratified/annular flow is an increasingly important area in two phase flow fluid research. The purpose of the research presented here was twofold. The first goal of this research was to characterize the wavy interface of the stratified flow, both in the spanwise direction and also through time. This was accomplished through the design and construction of a rectangular duct and the development of a visualization non-contact film thickness measurement method. The second goal of this research was to determine the effect of the addition of various concentrations of a drag reducing additive (DRA) on the wavy interface. This chapter includes the motivation for this research followed by background information on two phase flow. Finally, a list of specific objectives is presented along with an outline for the thesis.

### 1.1.1 Motivation

Horizontal two phase flow occurs in numerous engineering applications. Specifically, annular and stratified flow regimes occur in a wide variety of industrial situations including chemical processing, power generation, water supply systems and in long distance transfer pipelines for the petroleum industry. While the characteristics of annular and stratified flow regimes differ, the existence of a liquid film along the wall is a shared characteristic and it is the primary factor influencing frictional losses, heat transfer and corrosion of the pipe wall in these two phase flow regimes. It is also easier to experimentally study the stratified and stratified/annular regime than the more complex annular regime. Many predictive models for liquid hold up and pressure drop have been developed over the last couple of decades but there is not a single accepted analytical relationship. For this reason more research is required to fully understand the interface of the two phases in order to be able to more accurately predict pressure drop and heat and mass transfer.

In order to characterize the interface, an accurate and precise wavy film measurement technique was required. Despite that fact, there is no single measuring technique that satisfies all the specified requirements due to the complexity of the flow. Many of the more generally accepted methods of measuring wavy films are contact methods, usually needle contact (Mouza et al., 2000). These techniques have drawbacks, including the inability to measure very thin films due to the formation of a meniscus as well as the effect the probes have on the flow or for very thin probes, the effect the flow

has on the probes. Non contact methods of measuring wavy films including the light absorption method and the fluorescent method avoid the issue of flow disturbance; however, they are dependent on the limitations of the equipment used. Many of these methods were developed decades ago but were not pursued due to a lack of sensitive equipment. The development of more powerful lasers, more sensitive diodes and faster video cameras has led researchers to revisit many of these non-contact methods. Development of new methods is necessary in order to achieve a greater understanding of the wavy film in two phase flow.

While there has been a lot of research performed in understanding stratified flow in circular pipes, not much has been done recently in non-circular ducts. Stratified and annular flow patterns occur in steam boilers and chemical plants often in non circular, rectangular ducts. In addition many micro channel two phase flow applications occur in non-circular ducts. It has been known for quite some time that these flows exhibit somewhat different behavior than what occurs in circular ducts, including greater pressure drops and non uniform heat and mass transfer along the walls. This behaviour has also been found to scale well with microchannels (Shedd and Newell, 2004). More research in this area is required especially given the increase in nuclear power generation as the steam generators are often comprised of non circular flow passages.

Research into two phase horizontal stratified flow is also of specific interest to the petroleum industry. This flow pattern along with annular flow is often

found in production and in the transportation pipelines of gas/condensate and oil/gas systems. These pipelines typically cover between 10 km to 30 km but, can be as long as 100 km. Transporting the resources over such long distances causes large frictional losses especially as the velocities of the two streams increase. These losses decrease production resulting in additional costs and larger environmental impact. One solution to decrease the losses without increasing capacity or additional pumping power is through the addition of a long chain polymer to the liquid phase. While the effects of the addition of this polymer, also referred to as a drag reducing additive (DRA), have been widely known for years, the mechanism is still far from being understood (Manfield et al., 1999). Further research is necessary to determine the effect of the polymer on the interface of the fluids and on the waves and entrainment generated in the flow.

## 1.2 Background

### 1.2.1 Stratified Flow

The specific flow patterns that exist depend on the relative amounts of liquid and gas and the relative orientation of the pipe. Stratified flow occurs in a horizontal pipe at relatively low liquid and gas flow rates. This flow pattern can be characterized by two fluid streams flowing concurrently with the less dense fluid flowing above the denser fluid such that the interaction between the two fluids occurs only through its interface. A sketch of this flow pattern

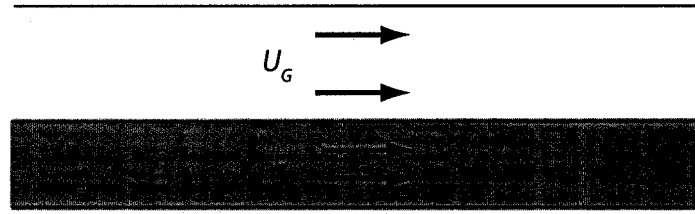


Figure 1.1: Depiction of stratified flow

is show in Figure 1.1.

Since the two fluid streams flowing together effect one another, one phase analytical equations for predictions of pressure drop are not applicable. The pressure drop of two phase flow generally consists of three components: frictional loss, momentum change and elevation change. For the work presented in this report, there is no acceleration so the pressure drop associated with the momentum change is zero as is the pressure drop associated with elevation change, since there was no change in height. Unlike the other two components, the frictional pressure drop depends strongly on the flow pattern in the pipe. Lockhart and Martinelli (1949) developed one of the first procedures for determining flow rate and pressure drop for two phase flow. It was based on the idea that the pressure drop of the two phases flowing simultaneously would be equal to the pressure drop of one phase flowing alone in the pipe multiplied by a factor.

$$\left(\frac{dp}{dx}\right)_{2-phase} = \Phi_s^2 \left(\frac{dp}{dx}\right)_s \quad (1.1)$$

The  $s$  in the equations denotes single phase, either gas or liquid. The

factor,  $\Phi_s$  depends on the phase being used and whether each phase is in the laminar or turbulent regime. This usually generates four curves for the different  $\Phi_s$  (turbulent-turbulent, turbulent-laminar, laminar-turbulent, laminar-laminar). This information is usually viewed in a figure where  $\Phi_s$  is shown as a function of the dimensionless pressure drop,  $X$ .

$$X = \left( \frac{(dp/dx)_L}{(dp/dx)_G} \right)^{0.5} \quad (1.2)$$

$X$  is generally referred to as the Lockhart-Martinelli parameter. Since the relationship they developed was applied to all flow regimes, depending on the flow condition this approach over predicted the pressure drop, sometimes by up to 100%.

In an effort to develop more accurate predictions of pressure drop and hold-up, Taitel and Dukler (1976) developed separate relations for different flow regimes. For the stratified flow regime they used the Lockhart-Martinelli parameter in their model. They indicated that the dimensionless liquid hold up,  $h_L/D$  was a unique function of the Lockhart-Martinelli parameter. This relationship was used to solve the momentum balance equations for stratified flow resulting in a better comparison with experimental data than the original relationship. For stratified flow the two phase momentum equations are written as follows.

$$-A_G \left( \frac{dp}{dx} \right) - \tau_{WG} P_G - \tau_i S_i = 0 \quad (1.3)$$

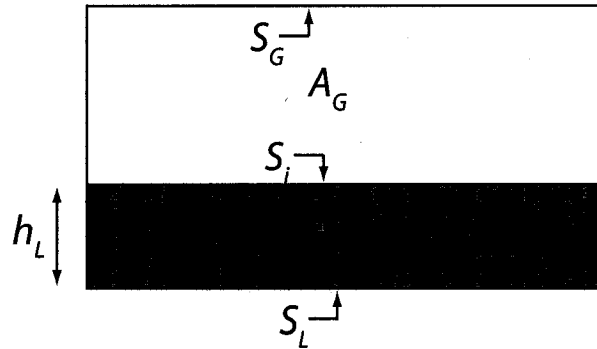


Figure 1.2: Front view of stratified flow in a rectangular channel

$$-A_L \left( \frac{dp}{dx} \right) - \tau_{WL} P_L + \tau_i S_i = 0 \quad (1.4)$$

Equation 1.3 represents a balance between the pressure forces on the gas space and the resisting stresses at the solid gas boundary and at the interface. Equation 1.4 represents a balance between the pressure forces caused by the drag of the gas on the liquid and the resisting stresses at the solid liquid boundary. The parameters for these equations are defined in Figure 1.2. The surface tension of the liquid is not included as it is negligible when compared with the inertial forces of the flow.

The two major assumptions used by Taitel and Dukler are:

1. The shear stress at the interface is equal to the shear stress of the gas at the wall.
2. The wall shear stress can be calculated using the fully developed flow correlation and using the proper hydraulic diameter.

Therefore the shear stresses are give by the following equations.

$$\tau_{WG} = f_G \frac{\rho_G U_G^2}{2} \quad (1.5)$$

$$\tau_{WL} = f_L \frac{\rho_L U_L^2}{2} \quad (1.6)$$

$$\tau_i = f_i \frac{\rho_G U_G^2}{2} \quad (1.7)$$

Much of the research done in the last few decades has been refining those two assumptions. Taitel and Dukler (1976) set  $f_i = f_G$  which only gives a good approximation if the interface is smooth. The difficulty arises in determining  $f_i$  once waves appear on the interface. Many researchers including Cheremisinoff and Davis (1979); Kowalski (1984); Andritsos and Hanratty (1987a) and more recently Ullmann and Brauner (2006) have developed models for predicting  $f_i$ . Other work by Vlachos et al. (1989) and Vlachos (2003) have included refining the predictions of  $\tau_{WG}$  and  $\tau_{WL}$  to account for the non-uniform shear stress around the pipe circumference.

### 1.2.2 Influence of Waves in Stratified Flow

The description of the waves that are present on the interface is important as they play a large role in determining the pressure drop and frictional losses of the system. In order to predict these parameters, a detailed understanding

of the waves is necessary.

The interface characteristics change primarily with changes in gas velocity. In round pipes, at low gas velocities the interface is unperturbed. As the gas velocity increases, an instability will form when the destabilizing pressure forces in phase with the wave slope overcome viscous dissipation (Andritsos and Hanratty, 1987b). The waves that form from this instability are usually described as two dimensional (2-D) waves and are identified by their small amplitude and regular appearance.

Further increases in gas velocity cause an imbalance between the destabilizing effects of the liquid inertia and pressure variations in phase with the wave height and the stabilizing effect of gravity (Andritsos and Hanratty, 1987b). This imbalance creates long wavelength, high amplitude waves to appear on the surface, more commonly known as roll waves.

If the gas velocity continues to increase, atomization occurs when the pressure variations over the waves is greater than the force of surface tension (Andritsos and Hanratty, 1987b). As the number of droplets increases, the droplets start to wet the upper surface of the pipe. This occurrence signifies the transition to annular flow. These transitions can be seen in Figure 1.3.

If the liquid flow-rate is increased, the waves on the surface will grow in amplitude until they wet the top surface. This signifies the transition to slug flow. All of the patterns that occur between an unperturbed gas-liquid interface to the onset of atomization are considered part of the stratified flow regime.

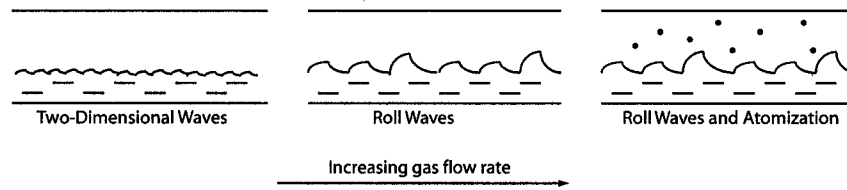


Figure 1.3: Sub-regimes of the stratified flow pattern

Typically, if the surface of the gas-liquid interface is unperturbed, it is described by researchers as smooth stratified. This occurs only for very low gas velocities. Once perturbations occur on the interface, the flow is considered to be in the wavy stratified regime Taitel and Dukler (1976). This regime can be broken down further into more specific classifications that exist based on different interface characteristics. Spedding and Spence (1993) performed research into refining the horizontal two-phase flow map for circular pipes and included flow sub-regimes within the stratified regime; stratified ripple, stratified roll wave and stratified roll wave and droplet. The stratified ripple regime consists of 2-D waves on the interface. The stratified roll wave regime corresponds to the initiation of large amplitude waves that occur at higher superficial gas velocities. Stratified roll wave and droplet occurs when the superficial gas velocity is large enough to rip liquid from the film and entrain it into the gas phase. In this regime the droplets may impinge on the upper surface of the pipe but it is not completely wetted.

Andritsos and Hanratty (1987b) described the surface waves that form at the interface in detail. The 2-D waves were described as having a small wavelength and a smooth and regular appearance across the interface. These

waves can be observed visually by light reflection from the liquid surface. The waves that occur at higher gas velocities are significantly different. These waves have a much greater amplitude and are much more irregular in nature. They also tend to have a steep wave front face and a relatively shallow rear wave face. These waves can also be viewed as surges in the liquid layer and are responsible for carrying large masses of fluid.

Many researchers including Mandhane et al. (1974), Taitel and Dukler (1976) and Andritsos and Hanratty (1987b) have empirically modeled the transition between one type of wave to another. According to Andritsos and Hanratty (1987b) the criterion for transitioning from an unperturbed surface to 2-D regular waves is given by

$$U_{GS} = 2\bar{\alpha} \left( \frac{(1 - \bar{\alpha})\nu_L(\rho_L - \rho_G)g}{(s\rho_G U_{LS})} \right)^{1/2} \quad (1.8)$$

The transition from 2-D waves to large amplitude waves is described in the flow map developed by Taitel and Dukler (1976) as the transition to wavy stratified flow. This is further described by Andritsos and Hanratty (1987b) where they used Kelvin Helmholtz (K-H) inviscid stability theory as a first approximation and some empirical data to fully describe the transition. The criterion is given as follows.

$$U_{K-H} = U_L + \left( \frac{k_m \sigma}{\rho_G} + \frac{g\rho_L}{k_m \rho_G} \right) \tanh(k\bar{H}) \quad (1.9)$$

$U_{K-H}$  is the first approximation for the gas velocity, given by K-H the-

ory, necessary to produce large amplitude waves. From equation 1.9  $k_m$  is the wavenumber predicted by (K-H) theory and is given by the following equation.

$$k_m = \left( \frac{\rho L g}{\sigma} \right)^{1/2} \quad (1.10)$$

Adjusting equation 1.9 with empirical information that takes into consideration the effect of liquid height and liquid viscosity gives the criterion for the superficial gas velocity necessary to cause the transition into the large amplitude wave regime for a given superficial liquid velocity.

$$U_{GS} = U_{K-H} \left( \frac{\theta_w}{\theta} \right)^{0.025} \left( \frac{1}{\tanh \left( \frac{k_m h}{10} \right)} \right)^{0.1} \left( \frac{1}{\alpha} \right) \quad (1.11)$$

For equation 1.11  $\theta$  is the dimensionless group used to take into consideration viscosity and  $\theta_w$  is the value for  $\theta$  if the liquid is water.

According to Andritsos and Hanratty (1987b), in rectangular channels another type of wave appears on the surface. At low gas velocities the unperturbed surface develops small two dimensional waves in the same manner that occurs in a circular pipe. However they exist only over a small range of superficial gas velocities. At higher gas velocities these waves break up on the surface into three dimensional waves that appear to have a pebble like appearance. With further increases in gas velocity, these waves change into the long-wavelength, large amplitude roll waves. Fukano et al. (1979) categorizes the transition from 2-D waves to 3-D waves as occurring when

the liquid flow rate is increased while the air flow rate is kept constant. They then describe another wave type that occurs when the gas flow rate is increased. These waves are labeled ripple waves and are described as having a more random appearance.

### 1.3 Research Objectives

The specific objectives of this research were as follows. The first was to design an apparatus and measurement method to properly visualize the interface surface. The method and apparatus were used to gather data over various superficial liquid and gas velocities and compare the results with previous studies. The second main objective of this work was to explore the effect on the waves of adding various concentrations of DRA to the liquid phase. This was done using the apparatus and method verified in the first objective.

### 1.4 Thesis Outline

The thesis is written in paper format with a bibliography at the end of each chapter. The first chapter presents an overview of the problem and some necessary background information. Chapter 2 presents further background information on the interface of stratified flow, a detailed description of the apparatus and the measurement method and discussion of those results. Chapter 3 describes the results of the effect of DRA on the wavy interface. Chapter 4 summarizes the work of this thesis and presents the conclusions

of the findings. A more condensed version of Chapter 2 will be submitted to the *Journal of Fluids Engineering* while a slightly modified Chapter 3 will be submitted to the *International Journal of Multiphase Flow*.

## BIBLIOGRAPHY

- Andritsos, N. and Hanratty, T. J. (1987a). Influence of interfacial waves in stratified gas-liquid flows. *AIChE Journal*, 33(3):444–453.
- Andritsos, N. and Hanratty, T. J. (1987b). Interfacial instabilities for horizontal gas-liquid flows in pipelines. *International Journal of Multiphase Flow*, 13(5):583–603.
- Cheremisinoff, N. P. and Davis, E. J. (1979). Stratified turbulent-turbulent gas liquid flows. *AIChE Journal*, 25:48–58.
- Fukano, T., Ishida, K., Morikawa, K., Nomura, H., Takamatsu, Y., and Sekoguchi, K. (1979). Liquid films flowing concurrently with air in a horizontal duct. *JSME*, 22:1374–1381.
- Kowalski, J. E. (1984). Wall and interfacial shear stress in stratified flow in a horizontal pipe. *AIChE Journal*, 33(2):274–281.
- Lockhart, R. and Martinelli, R. (1949). Proposed correlation of data for isothermal, two phase, two component flow in pipes. *Chemical Engineering Progress*, 45(1):39–48.

- Mandhane, J. M., Gregory, G. A., and Aziz, K. (1974). A flow pattern map for gas-liquid flow in horizontal pipes. *International Journal of Multiphase Flow*, 1:537–553.
- Manfield, P. D., Lawrence, C. J., and Hewitt, G. F. (1999). Drag reduction with additives in multiphase flow: a literature survey. *Multiphase Science and Technology*, 11:197–221.
- Mouza, A. A., Vlachos, N. A., Paras, S., and Karabelas, A. (2000). Measurement of liquid film thickness using a laser light absorption method. *Experiments in Fluids*, pages 355–359.
- Shedd, T. A. and Newell, T. A. (2004). Characteristics of the liquid film and pressure drop in horizontal, annular, two-phase flow through round, square and triangular tubes. *Journal of Fluids Engineering*, 126:807–817.
- Spedding, P. L. and Spence, D. R. (1993). Flow regimes in two-phase gas-liquid flow. *International Journal of Multiphase Flow*, 19(2):245–280.
- Taitel, Y. and Dukler, A. E. (1976). A model for predicting flow regime transitions in horizontal and near horizontal gas-liquid flow. *AIChE Journal*, 22(1):47–55.
- Ullmann, A. and Brauner, N. (2006). Closure relations for two-fluid models for two-phase stratified smooth and stratified wavy flows. *International Journal of Multiphase Flow*, 32(1):82–105.

Vlachos, N. A. (2003). Studies of wavy stratified and stratified/atomization gas-liquid flow. *Journal of Energy Resources Technology, Transactions of the ASME*, 125:131–136.

Vlachos, N. A., Paras, S., and Karabelas, A. (1989). Liquid-to-wall shear stress distribution in stratified/atomization flow. *International Journal of Multiphase Flow*, 23(5):845–863.

## CHAPTER 2

### MEASUREMENTS OF WAVY STRATIFIED FLOW

#### 2.1 Introduction

An experimental study was conducted to investigate the characteristic parameters of the interface of horizontal wavy stratified flow using a new measurement technique. There have been previous studies of horizontal wavy stratified flow in a pipe; however in an attempt to thoroughly characterize the wavy interface of the flow, a non-contact measurement technique using laser induced fluorescence and a high speed video camera was used. This system was capable of measuring temporal changes in the depth of the liquid layer as well as its changes in the cross-stream direction, in order to gather as much information on the interface as possible. Furthermore, in order to concentrate solely on the air-water interface, all experiments were performed in a rectangular channel, rather than a circular pipe.

The background section includes information on stratified flow and film thickness measurement techniques. Section 2.3 describes the apparatus de-

signed and built as well as the experimental setup. Section 2.4 discusses the methodology used to gather the necessary data. Section 2.5 contains the results from the experiments and interpretation and analysis of the data. Finally conclusions are given in section 2.6.

## 2.2 Background

### 2.2.1 Previous Research Work in Stratified Flow

A lot of the previous work in stratified flow has concentrated on refining the predictive models for pressure drop and liquid hold up. These models are based on the two phase stratified flow momentum equations given by:

$$-A_G \left( \frac{dp}{dx} \right) - \tau_{WG} P_G - \tau_i S_i = 0 \quad (2.1)$$

$$-A_L \left( \frac{dp}{dx} \right) - \tau_{WL} P_L + \tau_i S_i = 0 \quad (2.2)$$

The research has centered around determining the most accurate relationship for the interfacial shear stress usually by setting:

$$\tau_i = f_i \frac{\rho_G U_G^2}{2} \quad (2.3)$$

and developing models for the interfacial friction factor. There are numerous approximations, Ottens et al. (2001) discusses 22 different interfacial friction factor models by various researchers that were developed over the last couple

of decades. Most of the research; however, was confined to circular pipes and as such the approximations are not necessarily valid in other geometrical configurations.

Shedd and Newell (2004) performed a detailed study of stratified and annular flow through various geometries. They determined that the pressure drop in non circular pipes could be approximated by a function of the Lockhart-Martinelli parameter for turbulent-turbulent flow where the friction factor was defined as the non dimensional two phase pressure drop:

$$f = \frac{2\Delta p}{(L/D_h)(\rho_G U_{GS}^2)} \quad (2.4)$$

The relationship between  $f$  and the Lockhart-Martinelli parameter,  $X_{tt}$  developed by Shedd and Newell (2004) is as follows:

$$f = 0.251X_{tt} + 0.01 \quad (2.5)$$

where:

$$X_{tt} = \left(\frac{1-x}{x}\right)^{0.9} \left(\frac{\rho_G}{\rho_L}\right)^{0.5} \left(\frac{\mu_L}{\mu_G}\right)^{0.1} \quad (2.6)$$

$x$  is the mass quality of the flow and can be defined from the mass flow rates as:

$$x = \frac{\dot{m}_G}{\dot{m}_G + \dot{m}_L} \quad (2.7)$$

However, this empirical relationship has numerous limitations including larger errors with channels having aspect ratios, defined as  $\frac{W}{H}$ , larger than 1 and with the quality of the flow outside of 0.2 to 0.85.

Other work has concentrated on characterizing the interface in more detail in order to produce more accurate flow regime maps and predictive models. The classification of different wave types has been the subject of much research. In circular pipes Andritsos and Hanratty (1987b) classify three different sub-regimes in stratified flow. The unperturbed surface, 2-D waves and roll waves. Through semi-empirical relations they determined the transition requirements for each classification based on previous work by Mandhane et al. (1974) and Taitel and Dukler (1976).

The transition from 2-D waves to large amplitude waves has been described by numerous researchers including Mandhane et al. (1974), Taitel and Dukler (1976) and Andritsos and Hanratty (1987b). Andritsos and Hanratty (1987b) developed a relation for this transition using Kelvin Helmholtz (K-H) inviscid stability theory as a first approximation and empirical data to fully describe the effects of liquid height and liquid viscosity on the transition.

Paras et al. (1994) and Shi and Kocamustafaogullari (1994) both performed detailed experiments of the wavy interface in two phase stratified flow. Shi and Kocamustafaogullari (1994) studied the stratified interface in a 50.3 mm diameter pipe. They obtained data regarding the transition conditions for various interfacial wave patterns and examined wave parameters based on liquid and gas flow rates. These tests were done for superficial gas

velocities ranging from 0.85 m/s to 31.67 m/s and superficial liquid velocities ranging from 0.014 m/s to 0.127 m/s. Results indicated that gas velocity was the major factor affecting film thickness, dominant wave frequencies and the transition from stratified flow to stratified-annular flow. They discovered that the average film thickness decreased with increasing superficial gas velocity. This decrease was more gradual in the roll wave regime than in the stratified ripple regime. Dominant wave frequency was found to be a strong function of  $U_G$  and was constant around 2-5 Hz for the roll waves.

Paras et al. (1994) also performed work on characterizing the stratified interface in a 50.8 mm diameter pipe. In addition to film thickness and wave frequency they also measured RMS wave heights, large wave amplitudes and wave intermittency. As with Shi and Kocamustafaogullari (1994), Paras et al. (1994) noted that dominant frequency was strongly dependent on gas velocity. They found that for gas velocities greater than  $U_G = 10$  m/s, the wavy stratified regime enters the stratified-atomization regime. They showed that this regime appeared to be characterized by disturbance waves with a frequency around 1 Hz.

### 2.2.2 Film Thickness Measurement Techniques

In order to properly characterize the in gas-liquid interface an effective method of measuring the instantaneous liquid height is necessary. Due to the complexity of two phase stratified or annular flow, there is no universal standard for measuring the film height (Mouza et al., 2000). Available techniques are

often grouped into contact and non-contact methods. Contact methods including wire probes and the capacitance method have been used for decades and as such have undergone extensive improvements. Non-contact methods, while having the advantage of not causing disturbances in the flow, tend to rely on the accuracy and sensitivity of very specific equipment and as such have not been widely used until recently.

One of the most common contact methods is the use of wire probes to measure film thickness. This method is described by Brown et al. (1978) and functions as follows. Two electrodes are mounted into the wall of the apparatus and point into the flow. The conductance between the electrodes is proportional to the height of the film and the distance between the probes. This method has been widely used by numerous researchers including Miya et al. (1971); Andritsos and Hanratty (1987a); Paras et al. (1994) and Shi and Kocamustafaogullari (1994). However it is inadequate for measuring very small liquid heights due to the formation of a meniscus around the wire (Mouza et al., 2000). There is also a small problem with a time lag in a wavy film since as a wave passes by the probe and the height level decreases a thin layer of liquid may still adhere to the probe causing an error in recorded height. In addition, this measurement system requires an electrically conducting fluid and the calibration required for the wire probes can be tedious.

A similar method based on the same principle as the wire probes is the the capacitance method described by Ozgu et al. (1973). However, instead of

probes, two electrodes are placed flush in the apparatus wall such that they do not disturb the flow. Another advantage of this system is that the fluid is not required to be electrically conducting. However, the response of the system is not linear and it is only capable of point measurements.

One class of non-contact measurement techniques that have been revisited more recently is the light absorption method. Studies of this method have been done in an attempt to eliminate some of the disadvantages produced by the conductance methods. The light absorption method is based on the principle that for a fixed dye concentration the light absorption is related to the height of the film through Lambert's law. Using a small diode laser and a photodiode the instantaneous film height can be recorded (Mouza et al., 2000). The sensitivity and accuracy of the system is dependent on the quality of the laser and the frequency response of the photodiode. The main drawback of the system is reflected and/or refracted light can sometimes reach the photodiode causing errors in the height measurements.

## **2.3 Apparatus**

### **2.3.1 Experimental Apparatus**

As mentioned previously, one of the objectives of the work was to characterize the gas-liquid interface. For this reason it was decided that a transparent duct of rectangular cross-section would be used. This would allow for the determination of the interface characteristics while keeping the interface length

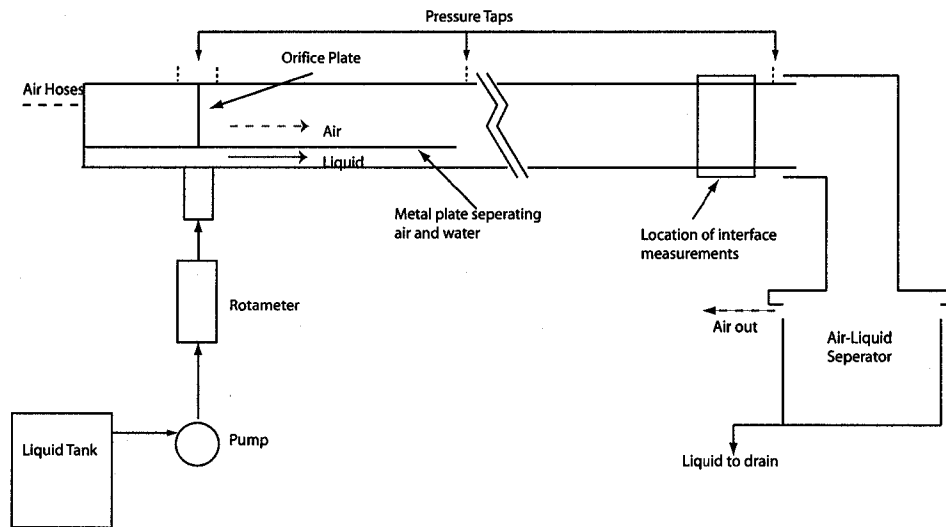


Figure 2.1: Schematic of the experimental apparatus

constant. The other benefit of the decision to use a rectangular cross-section was that it reduced the the variables for designing and implementing the measurement method.

The experimental apparatus is shown in Figure 2.1. It was braced by five metal supports in order to prevent vibrations caused by the moving fluids. During setup it was positioned carefully to avoid sloping in either the longitudinal or lateral directions.

The apparatus was constructed from four pieces of polished acrylic each 2.5 m in length. The four pieces were attached together to create a rectangular duct with a cross-section of 25.4 mm by 50.8 mm. The two sides of the apparatus were attached to the floor by interspaced screws and pins, 17 of each. Each of the pins and screws were attached to the sides of the

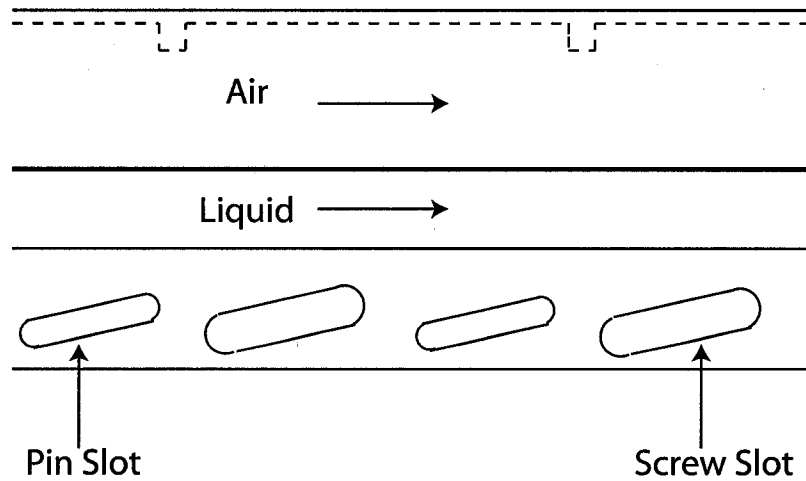


Figure 2.2: Schematic of the section of the apparatus depicting the screw-slot system

apparatus through a 25 mm slot angled at 14 degrees to the horizontal. This configuration allowed the floor height to be adjusted by loosening the screws and can be seen in Figure 2.2. In order to minimize interference in the flow, the sides were mounted flush with the floor. The top of the apparatus was attached with 29 screws on each side and sealed with two elastomer sealing bands in order to prevent any air from escaping.

Air entered the apparatus at one end through two 0.75 ID air hoses which were attached to a brass end piece. Water entered from the bottom of the apparatus through two 0.75 inner diameter hoses positioned at 7.4 diameters and 10.4 diameters downstream from the air inlet. The system was designed with two liquid inlets to try to achieve a more uniform liquid profile. The liquid inlet opened up into a shallow basin where the water collected before moving downstream into the rest of the apparatus via a shallow ramp (3.6

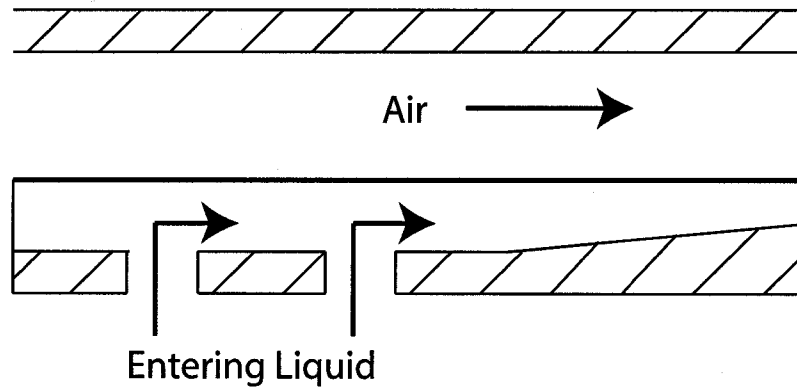


Figure 2.3: Schematic of apparatus floor showing the water inlet section

degrees to the horizontal). This occurred 18 diameters downstream from the air inlet. This is shown in Figure 2.3.

The air and water were separated by a 0.8 mm thick aluminum plate for 45 diameters before mixing to ensure that both streams were fully developed. While the area of the air flow section remained constant, the area of the water flow section could be adjusted using the screw-slot system. The system allowed for thicknesses between 2.5 mm and 5 mm. For this report all experiments were performed with the minimum inlet water thickness of 2.5 mm.

The variables controlled in the experiment were the air and water flow rates. Air was supplied by compressed air and was adjusted using a valve in the air line. A rectangular orifice plate located 12 diameters downstream from the air inlet measured the incoming air flow rate. Pressure taps for the orifice plate were attached to pressure transducers which were wired to demodulators and the outputs recorded by a data acquisition system. Water

was pumped from a 300 litre tank using a moving vane positive displacement pump. The pump was driven by a variable speed motor to allow for water flow rate control. A rotameter of range 0-0.000126 m<sup>3</sup> was located at the water inlet and used to measure the flow rate of the water.

Atmospheric pressure was measured by a pressure transducer and recorded by the the data acquisition system at the beginning of every test.

The pressure drop of the system was measured over a test section of one metre. The two pressure taps were located over the centerline of the duct and were attached to a variable capacitance diaphragm pressure transducer which was wired to a demodulator and its output recorded by the data acquisition system. All interface measurements were made 30 diameters downstream from the mixing point using laser induced fluorescence and a high speed video camera. At the end of the apparatus the gas and liquid were separated by a gas-liquid separator.

The separator was designed such that it was open to the atmosphere and therefore negligible back pressure was enforced on the apparatus. The end of the apparatus was situated just inside of the inlet of the separator remaining open to the atmosphere. The two fluid streams were drawn downwards towards the body of the separator. A small gap around the neck and the body of the separator allowed the air to escape and the liquid to be drawn further into the tank. The liquid was then drained from the separator and disposed.

### 2.3.2 Orifice Meter Calibration and Flow Verification

The orifice plate was constructed from aluminum and designed using ASME orifice plate specifications. It had a rectangular cross section of 20.3 mm by 40.6 mm which corresponded to a ratio of diameters,  $\beta$ , of 0.8. The orifice plate specifications can be found in Appendix A.

Verification of the accuracy of the orifice plate was done to ensure that it was properly installed since improper installation can cause up to a 20% error (Humphreys, 1987). A pitot tube was placed at the end of the apparatus and attached to a Mark II Dywer Instruments manometer with a range of -0.254 cmH<sub>2</sub>O to 15.24 cmH<sub>2</sub>O with variable resolution. The pitot tube was used to determine the velocity at numerous points over the cross section and summed in order to calculate the flow rate. A 16 point Centroids of Equal Area distribution integration method was used. This calculated flow rate was then compared to the flow rate determined by the orifice plate. Three different air flow rates were measured, 0.0150 m<sup>3</sup>/s, 0.0215 m<sup>3</sup>/s and 0.0263 m<sup>3</sup>/s which correspond to superficial velocities of 12 m/s, 16 m/s and 20 m/s respectively. There was less than a 4% difference between the values calculated from the orifice plate and those measured by the pitot tube. These measurements also illustrated the nature of the air velocity profile and the fully developed flow assumption in one phase. These results can be seen in Figure 2.4.

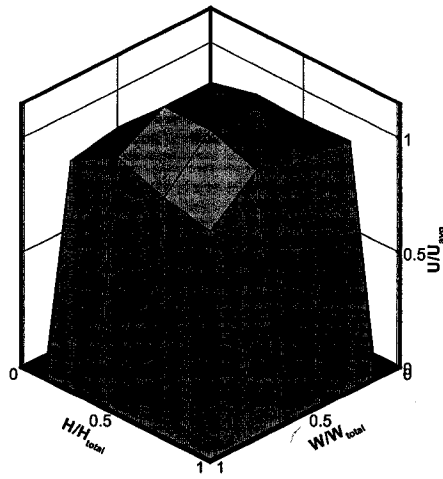


Figure 2.4: Verification of orifice plate calibration

### 2.3.3 Rotameter Calibration

The rotameter used had a range of  $0 - 1.26 \times 10^{-4} \text{ m}^3/\text{s}$  with a resolution of  $1.26 \times 10^{-5} \text{ m}^3/\text{s}$ . It was calibrated using a 10 liter container and a timer. The instrument was tested at at four different flow rates,  $3.15 \times 10^{-5} \text{ m}^3/\text{s}$ ,  $6.31 \times 10^{-5} \text{ m}^3/\text{s}$ ,  $9.46 \times 10^{-5} \text{ m}^3/\text{s}$  and  $1.26 \times 10^{-4} \text{ m}^3/\text{s}$ , three times each. Although the greatest uncertainty was observed at  $1.26 \times 10^{-4} \text{ m}^3/\text{s}$ , that value was not used since the maximum liquid flow rate used in the experiment was  $6.31 \times 10^{-5} \text{ m}^3/\text{s}$ . Based on that information the uncertainty related to the flow rate measurement was determined to be  $\pm 6.94 \times 10^{-6} \text{ m}^3/\text{s}$  or 7.3% of full scale.

### 2.3.4 Laser Set-up

An Ion Laser Technology (ILT) Model 5500 A Argon-Ion laser 100 mW laser was used to illuminate the liquid phase. It was operated at single line mode which produced a 0.82 mm diameter beam at a 488 nm wavelength. The laser was positioned such that the beam was 25 cm from the bottom of the apparatus.

In order to create a laser sheet, the beam was passed through a convex collimating lens with a 30 cm focusing length. Since the bottom of the apparatus was 25 cm above the laser optics, the use of this lens focused the beam to a point at approximately the area where measurements were made. The focused beam then passed through a cylindrical lens to create a laser sheet. A mirror was placed 2 cm in front of the cylindrical lens and angled at

approximately 30 degrees. The laser sheet was directed upwards such that it was perpendicular to the mean flow direction, cutting through the cross-section of the duct. The size of the cylindrical lens was chosen such that at the height of the apparatus the length of the laser sheet was slightly smaller than the width of the channel. Since a cylindrical lens expands the beam in one direction only, the thickness of the laser sheet remained the same as the original radius. The setup can be seen in Figure 2.5.

In order for the laser light sheet to be clearly visible through the liquid, sodium fluorescein dye (commercial name Uranine) was added to the water. At the concentration used the dye turned the water a light green, but fluoresced bright green, 565 nm, when it came in contact with the laser light. This phenomenon created a light sheet that clearly illuminated a cross-section of the water flowing in the duct.

### 2.3.5 Camera Set-up

A Photron Fast-Cam 8-bit colour high speed video camera was used for the filming. It was positioned underneath the apparatus such that the lens was approximately 26 cm from the bottom of the apparatus and was pointed at a 45 degree angle to the test section. This set up can be see in Figure 2.6. All images were taken at a resolution of 240 pixels by 256 pixels. In order to assure that the camera remained in the same position for every test a small black mark was placed on the underside of the apparatus. This created a small discontinuity in the fluoresced laser line. The setup was adjusted such

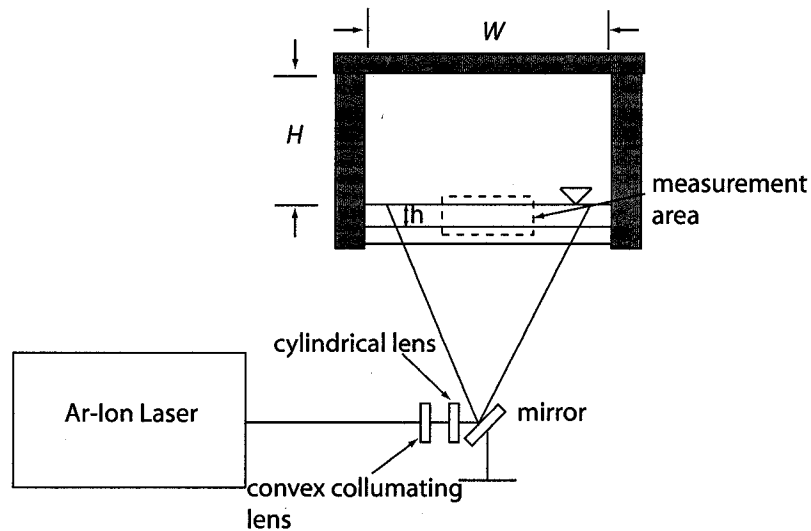


Figure 2.5: Front view of apparatus including the position of the laser and associated optics.  $H=25.4$  mm,  $W=50.8$  mm and  $h$  is the height of the liquid film.

that the one corner of the discontinuity was always at location (221,166) on the photograph. This is shown in Figure 2.7.

## 2.4 Measurement Method

In order to gather all the necessary data, multiple measurement systems were used. The pressure and velocity measurements were obtained by pressure transducers and recorded by the data acquisition system. For the interface measurements, a technique using laser induced fluorescence and high speed video recording was used. The data were acquired by the video camera and the information was determined through post processing of the images.

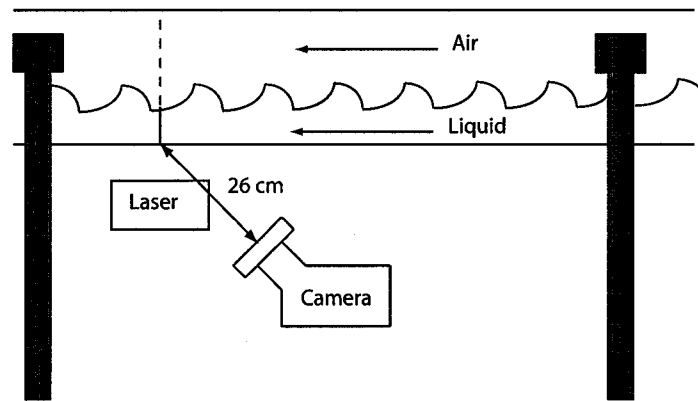


Figure 2.6: Side view of the apparatus including the position of the camera

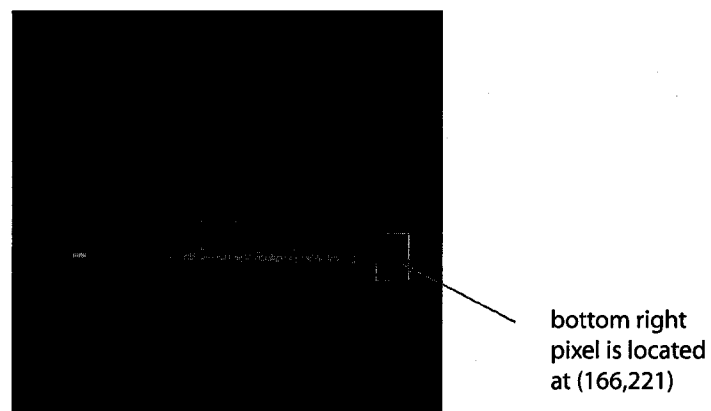


Figure 2.7: Discontinuity in the laser sheet to ensure repeatable measurements

### 2.4.1 Pressure and Flow Rate Measurements

A test run consisting of dry air only was completed at the start of the test in order to verify the state of the pressure transducers. At the beginning of every run, the air was switched on first and the valve adjusted to achieve the desired flow rate. The water was then initiated and the pump adjusted to give the desired flow rate. The pressure drop measurements and flow measurements were made after the system had achieved steady flow which was defined as when the mean parameters were constant, a change of less than 1%, over time. Data from the pressure transducers were recorded for at least 15 seconds at a sampling frequency of 1000 Hz. The liquid flow rate determined from the rotameter and was taken as an average over a one minute interval.

### 2.4.2 Interface Measurements

In order to characterize the interface, a method using laser induced fluorescence and high speed videography was developed to determine the height of the liquid film spanwise across the channel.

The setup of the laser in section 2.3.4 created a fluorescent light sheet that generated a definite dividing line between the air and water surface. Using the camera setup described in section 2.3.5 the illuminated laser sheet was filmed creating images where the instantaneous interface along the spanwise direction was clearly defined.

The spatial fluctuations were captured by the high speed video camera

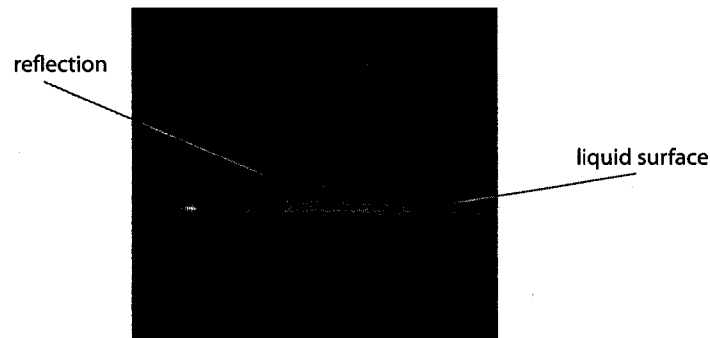


Figure 2.8: Example of reflection of laser light that occurs on the interface surface. A noticeable difference in the intensity between the actual image and the reflection can be seen due to the use of a polarizing filter.

in order to determine liquid height and dominant frequency of the waves. However certain problems were identified, the most influential one being the reflections. The laser light reflected off of all interfaces; air-acrylic, acrylic-water and water-air. Since the reflections off the solid-fluid interfaces occurred perpendicular to the mean flow direction they did not appear on the images since the camera was pointed at a 45 degree angle. However since the air-water interface was wavy, reflections off that interface occurred in all directions, many of which appeared on the images. This effect made it difficult to determine the actual height of the film. In order to reduce the intensity of the reflections, a linear polarizing filter was attached to the camera. While this increased the difference in intensity between the actual images and the reflections, post-processing was required to completely remove the reflections from the images. An example of a typical reflection that required post-processing to remove it is shown in Figure 2.8.

Post processing was done as follows. Since the predominant colour in the photographs was green, the blue and red colours in each pixel were set to zero, transforming them to black. This effectively converted the frames from true colour RGB to grayscale. Due to the use of the polarizing filter, the reflections that occurred in the photographs were not as bright as the actual image; therefore, a thresholding technique was used to remove them. For each column in the frame the maximum intensity value was determined and any pixel that had a value less than 75% of that maximum value had their value reassigned to zero thereby showing up black on the image. The image was then converted to a binary image for easier manipulation. At this point the image was completely black except for the white zone showing the thickness of the liquid layer. Since the laser sheet did not extend all the way across the duct and the light concentration using a cylindrical lens is not uniform, it was decided to concentrate only on an area in the centre of the duct. Starting at horizontal pixel location 99 to horizontal pixel location 190, the thickness of the white line was determined, in pixels, by moving from the bottom of the image upwards. This entire process is shown in Figure 2.9.

In certain images it appeared that the light reflected off a particle in the water as a bright flash of light would appear on the image. This distorted the image and the usual way of determining the difference between the image and the reflection could not be used. In these cases the image was discarded and the data estimated using a linear interpolation between previous and subsequent images. No more than 15 interpolations were applied for a given

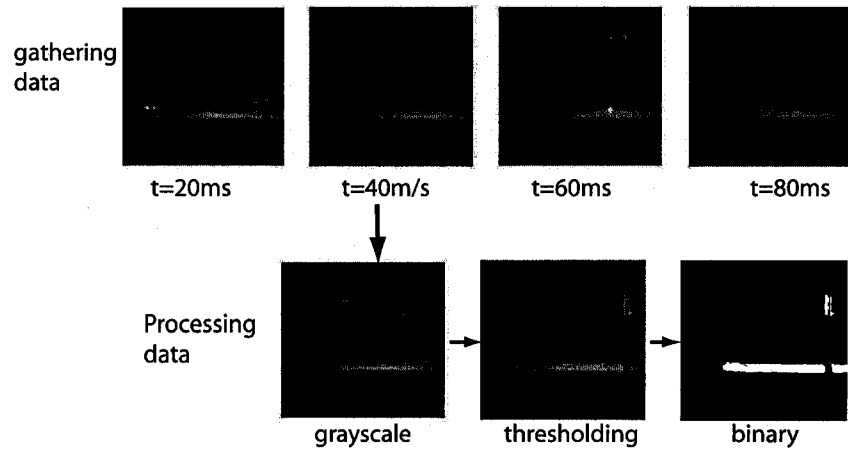


Figure 2.9: Image processing procedure

test so at maximum only 0.75% of any run was interpolated data.

A grid system was used in order to convert the pixel height to a height in millimeters. The grid used consisted of a series of 1 mm by 1 mm squares and was cut to be the same size as the cross section of the experiment. The grid was placed at the same position as the laser sheet and was illuminated by an LED light source. It was filmed at the same sampling rate as the experiments in order to reproduce the same conditions. From the image of the grid it was determined there was a resolution of 12 pixels/mm with an uncertainty of  $\pm 1$  pixel. Using this conversion, the instantaneous height of the film was calculated over a 7 mm distance in the centre of the duct.

In order to determine the accuracy and precision of the system, a static calibration was performed. Three different liquid levels were measured using a digital caliper and compared with the height level determined from the video. Using this method an uncertainty value of  $\pm 0.6$  mm was calculated.

However, using the calipers injected more error into the measurement due to the setup and method. Therefore this value was not taken as the uncertainty value for the height measurement. Instead the resolution of the method,  $\pm 0.08\text{mm}$  was used.

The filming was done at a 1000 frames/s over 2.5 seconds. However, due to the high sampling rate and the resolution of the system some high frequency noise was introduced into the film thickness results. This noise was removed through use of a low pass digital filter. Based on previous studies demonstrating that the dominant wave frequencies for the flow conditions occurred well below 100 Hz, an Equiripple low pass digital filter with a 150 Hz cut-off was applied to the data. Complete specifications of the digital filter can be found in Appendix B.

In order to verify that 2.5 seconds was a long enough window time to record data, data for a specific flow condition was recorded over 2 seconds, 5 seconds and 8.7 seconds (the largest the buffer could hold) and compared. The largest difference in average film height, RMS wave heights and large amplitude wave heights recorded over 2.5 seconds and recorded over 8.7 seconds was less than 7%, but the typical error was about 2%. This comparison can be seen in table 2.1

However, there was a very large difference in the frequency results between 2 seconds and 8 seconds. It was decided that this error was unacceptable and that a longer sampling time was required. In addition, since it could be seen that the dominant frequencies of the waves occurred around 5-20 Hz. For

Table 2.1: Interface data collected at  $U_{GS}=16$  m/s and  $U_{LS}=0.06$  m/s over 2 seconds, 5 seconds and 8.7 seconds

Time(seconds)	$\bar{h}$ (mm)			$h_{RMS}$ (mm)			dH (mm)		
	A	B	C	A	B	C	A	B	C
2	1.351	1.241	1.096	0.322	0.361	0.391	1.508	1.857	2.137
5	1.331	1.218	1.096	0.336	0.368	0.398	1.547	1.996	2.063
8.7	1.337	1.220	1.108	0.332	0.372	0.406	1.510	1.909	2.014
Percent error between 2 and 8.7 seconds	0.99	1.67	1.12	3.09	2.87	3.79	0.15	2.68	6.10

this reason it was decided that the sampling rate could be reduced to 500 frames/s reducing the digital memory required. For wave frequency analysis, the interface was recorded at 500 frames/s for 8 seconds. This enabled the collection of more data which in turn allowed for a better signal-to-noise ratio.

### 2.4.3 Repeatability

Repeatability tests were performed to evaluate the reproducibility of the experiments. Two separate tests were performed, one for  $U_{GS}=14$  m/s,  $U_{LS}=0.04$  m/s and one for  $U_{GS}=18$  m/s,  $U_{LS}=0.07$  m/s. Each test was performed five times. The results can be seen in Table 2.2.

The results show small variation in the results. The maximum variation recorded was 5.1% demonstrating the repeatable nature of the experiment.

Table 2.2: Summary of the repeatability tests. The average heights and RMS wave height results are for the centre of the duct.

Parameter	Run 1	Run 2	Run 3	Run 4	Run 5	Variation (%)
$Q_L$ (m <sup>3</sup> /s)	$5.05 \times 10^{-5}$	NA				
$Q_G$ (m <sup>3</sup> /s)	0.0181	0.0181	0.0182	0.0183	0.0179	0.82
$P_{upstream}$ (Pa)	94512.9	94508.6	94509.6	94509.6	94508.3	0.0
$\Delta P$ (Pa)	98.0	97.3	97.6	95.4	95.0	1.42
$\bar{h}$ (mm)	1.09	1.07	1.06	1.07	1.10	1.55
$h_{RMS}$ (mm)	0.35	0.32	0.33	0.35	0.32	5.1
$Q_L$ (m <sup>3</sup> /s)	$8.83 \times 10^{-5}$	NA				
$Q_G$ (m <sup>3</sup> /s)	0.0233	0.0234	0.0233	0.0233	NA	0.19
$P_{upstream}$ (Pa)	94653.8	94660.6	94655.0	94660.3	NA	0.0
$\Delta P$ (Pa)	195.3	196.8	196.4	195.8	NA	0.35
$\bar{h}$ (mm)	1.14	1.16	1.16	1.16	1.10	0.92
$h_{RMS}$ (mm)	0.39	0.38	0.40	0.39	0.33	2.4

#### 2.4.4 Systems and Test Conditions

Tests were carried out in the air-water system. Superficial air velocities ranging from 12 m/s to 20 m/s and superficial liquid velocities from 0.04 m/s to 0.07 m/s were used. For this setup, these conditions fell within the wavy stratified flow regime. Since the separator was open to the atmosphere, the experiment was run at basically atmospheric pressure and as such viscosities of air and water were taken at standard atmospheric temperature and pressure.

## 2.5 Results and Discussion

Experiments were performed according to the method outlined in section 2.4 and at the velocities discussed in section 2.4.4. The results discussed here include interfacial wave classifications, film thickness results, RMS wave heights, pressure drop results and dominant wave characteristics. Comparisons with previous work in the field of interfacial measurements of stratified flow are also included in this section.

### 2.5.1 Interfacial Waves

From the digital images taken of the interface, instantaneous height measurements across a 7 mm spanwise distance in the centre of the duct were calculated for each experimental run. A surface plot of each test was generated with the data gathered. An example from one test can be seen in Figure 2.10. Since atomization occurred only at the highest superficial velocities and even then it was negligible, it was assumed that all the liquid remained flowing in the liquid film.

As mentioned in section 2.4 a 100 Hz low pass digital filter was applied to the data to remove the high frequency noise. A comparison of the two traces can be seen in Figure 2.11. A summary of the analysis performed on the interfacial data collected is presented in Table 2.3.

Observations and quick estimates using the flow map from Taitel and Dukler (1976) demonstrated that the experiments were performed in the

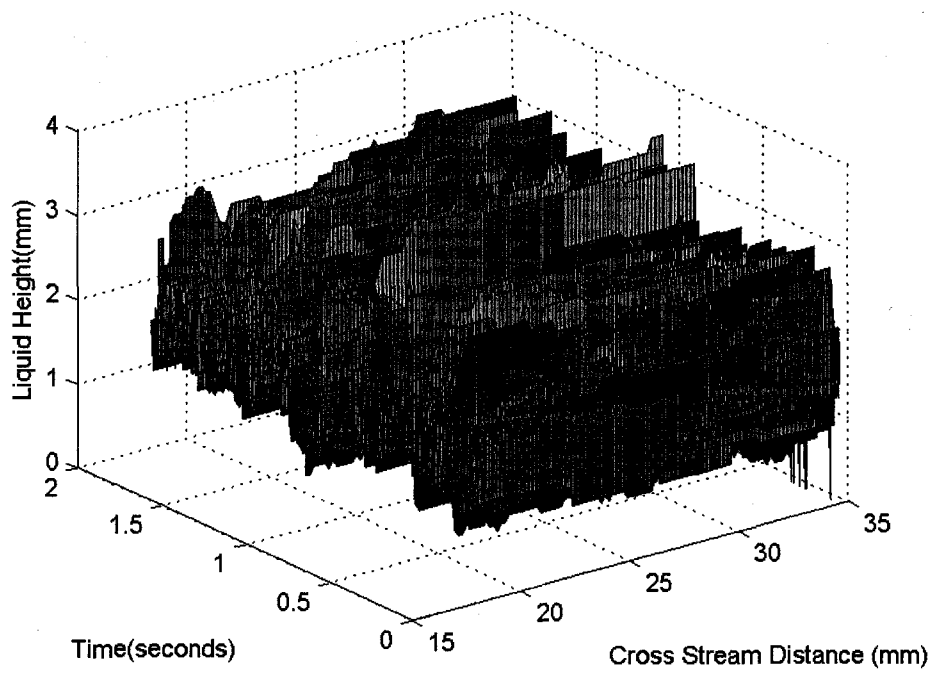


Figure 2.10: Surface plot of film height for  $U_{GS} = 12m/s$  and  $U_{LS} = 0.07m/s$ .

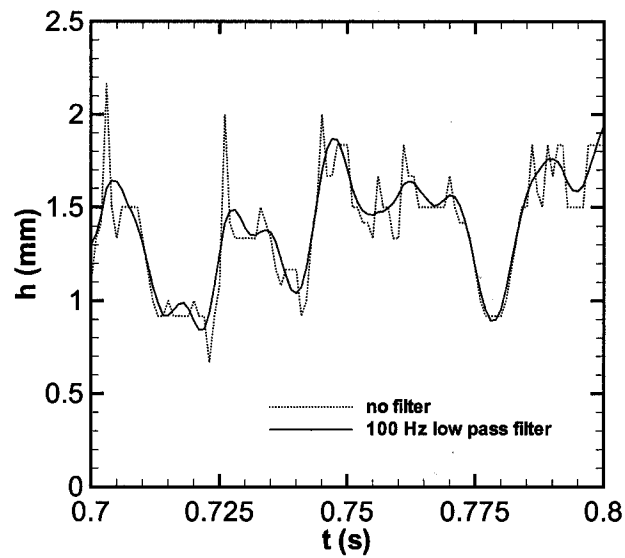


Figure 2.11: Result of using the 100 Hz low pass filter on the data. It can be seen that the use of the low pass filter removes the high frequency noise from the results.

Table 2.3: A summary of the interface data collected with the laser-camera setup.

$U_{LS}$ (m/s)	$U_{GS}$ (m/s)	$\bar{h}$ (mm)			$h_{RMS}$ (mm)			dH (mm)		
		A	B	C	A	B	C	A	B	C
0.04	12	1.40	1.28	1.15	0.28	0.32	0.31	1.25	1.53	1.66
0.04	14	1.27	1.20	1.17	0.28	0.34	0.40	1.50	1.90	2.05
0.04	16	1.17	1.08	1.06	0.31	0.34	0.40	1.50	1.76	2.18
0.04	18	1.12	1.03	1.02	0.28	0.31	0.39	1.49	1.69	2.05
0.04	20	1.05	0.98	0.99	0.31	0.37	0.43	1.53	2.04	2.24
0.05	12	1.50	1.41	1.33	0.31	0.35	0.40	1.22	1.59	1.83
0.05	14	1.34	1.25	1.23	0.39	0.34	0.40	1.36	1.67	1.99
0.05	16	1.28	1.18	1.16	0.31	0.34	0.39	1.48	1.75	1.97
0.05	18	1.19	1.10	1.10	0.28	0.32	0.41	1.39	1.77	2.15
0.05	20	1.13	1.05	1.06	0.30	0.34	0.43	1.63	1.88	2.17
0.06	12	1.57	1.48	1.40	0.29	0.36	0.40	1.21	1.70	1.81
0.06	14	1.43	1.33	1.28	0.31	0.36	0.41	1.41	1.80	2.06
0.06	16	1.33	1.22	1.20	0.31	0.35	0.43	1.42	1.81	2.10
0.06	18	1.27	1.18	1.19	0.29	0.33	0.41	1.45	1.73	2.02
0.06	20	1.21	1.17	1.17	0.30	0.38	0.44	1.53	2.03	2.05
0.07	12	1.55	1.46	1.42	0.33	0.39	0.45	1.36	1.69	1.89
0.07	14	1.44	1.33	1.29	0.34	0.39	0.44	1.50	1.77	2.08
0.07	16	1.41	1.26	1.20	0.34	0.38	0.42	1.50	1.94	1.93
0.07	18	1.32	1.24	1.21	0.32	0.38	0.42	1.42	1.93	2.04
0.07	20	1.28	1.21	1.20	0.33	0.38	0.44	1.52	1.83	2.20

wavy stratified regime.

According to the criterion for transitioning to large amplitude waves by Andritsos and Hanratty (1987b) discussed in Section 1, roll waves should occur around  $U_{GS} = 11$  m/s at the lowest superficial liquid velocity tested ( $U_{LS} = 0.04$  m/s). However, for the lowest superficial gas and liquid velocities

tested ( $U_{GS} = 12\text{m/s}$  and  $U_{LS} = 0.04\text{m/s}$ ) the waves on the surface do not appear to be the large amplitude roll waves. Instead they resemble the 3-D pebbled waves described by Fukano et al. (1979).

From Figure 2.12, it can be seen that while the amplitude of the waves is not yet that large, they are beginning to show some irregularity and small surges can be observed. As the superficial gas velocity increases, the waves on the interface transition fully to the roll wave regime. At low superficial liquid velocities this occurs at a superficial gas velocity of 14 m/s as can be seen in Figure 2.13. For increased superficial liquid velocity this transition occurs at lower superficial gas velocities. At a superficial liquid velocity of 0.07 m/s, roll waves were present at a superficial gas velocity of 12 m/s.

In Figure 2.14 the dimensionless time averaged film height,  $\bar{h}/D_h$ , is plotted as a function of superficial gas velocity. The values are fairly constant with changes in superficial velocity. There was only a slight decrease in average film height with increasing superficial velocity and a slight increase with increasing superficial liquid velocity. In studies done with circular pipes, (Shi and Kocamustafaogullari, 1994), there was a much greater dependence on superficial velocities than demonstrated here.

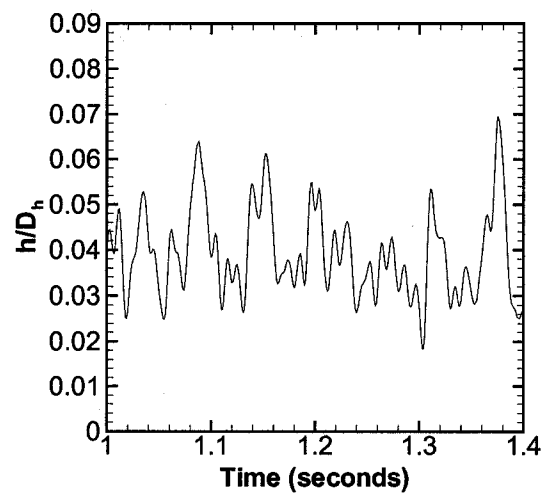


Figure 2.12: Dimensionless instantaneous film height for  $U_{GS} = 12m/s$  and  $U_{LS} = 0.04m/s$ . The waves display behavior that suggests that they are not yet large amplitude roll waves, but instead appear to be similar to 3-D pebbled waves.

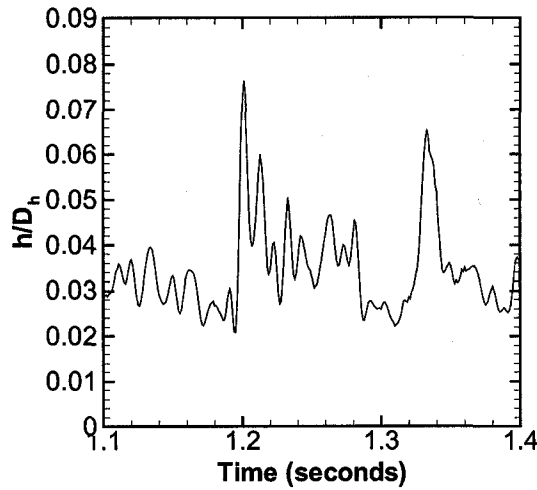


Figure 2.13: Dimensionless instantaneous film height for  $U_{GS} = 14\text{m/s}$  and  $U_{LS} = 0.04\text{m/s}$ . The waves are in the large wave amplitude regime as can be seen from the steep front face and relatively longer rear face of the waves.

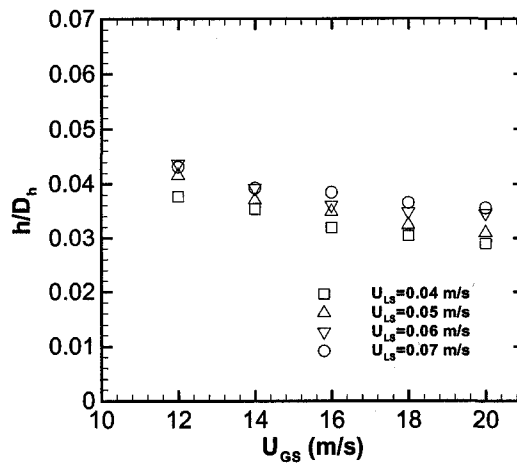


Figure 2.14: Effect of gas and liquid superficial velocities on dimensionless time averaged film height. The values appear to be fairly insensitive to changes in superficial velocities.

### 2.5.2 RMS Wave Heights

One way to characterize the nature of the wavy flow is to calculate the RMS values of the film thickness traces. The RMS value can be defined as:

$$h_{RMS} = \sqrt{\frac{1}{n} \sum_{i=1}^n h_i^2} \quad (2.8)$$

It can be seen in Figure 2.15, that the RMS wave height values seem to increase with increasing superficial liquid velocity, but appear to be independent of superficial gas velocity. Work done by Paras et al. (1994) which was in a circular pipe, demonstrated a definite trend of RMS wave heights decrease with increasing gas velocity.

RMS wave heights can also be related to the mean large wave amplitude,  $dH$ . The mean large wave amplitude was calculated as the largest difference between crest and trough,  $\Delta h$ , over a 200 millisecond time section for a given cross-stream location. These values were then averaged to give the mean large wave amplitude,  $dH$ , for a set of given conditions. The definition of  $\Delta h$  can be seen in Figure 2.16.

From Figure 2.17, it can be seen that  $dH$  is a linear function of the RMS wave heights with  $dH = 4.89h_{RMS}$  providing the best fit line. This trend was also observed by Paras et al. (1994) except that for their data the relationship discovered was  $dH = 2\sqrt{2}h_{RMS}$ . This suggests that the waves seen for this configuration are slightly different than what is seen in a circular pipe.

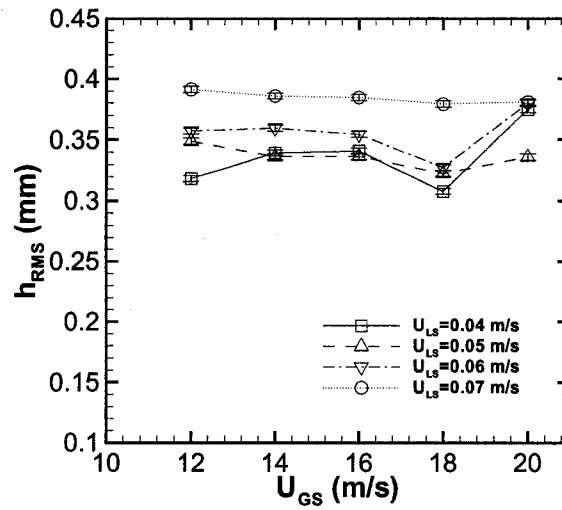


Figure 2.15: Effect of gas and liquid superficial velocities on RMS film heights. The values appear to be fairly insensitive to changes in superficial velocities.

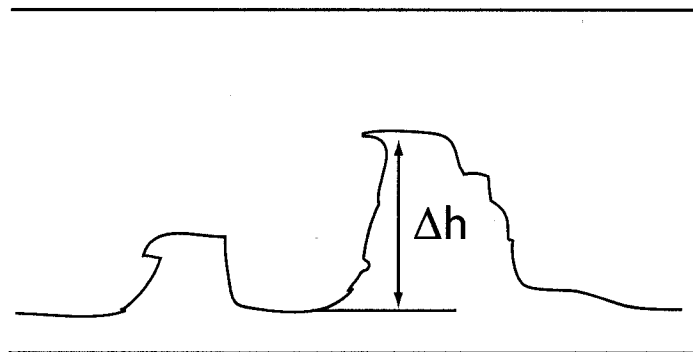


Figure 2.16: Definition of wave parameter  $\Delta h$ .

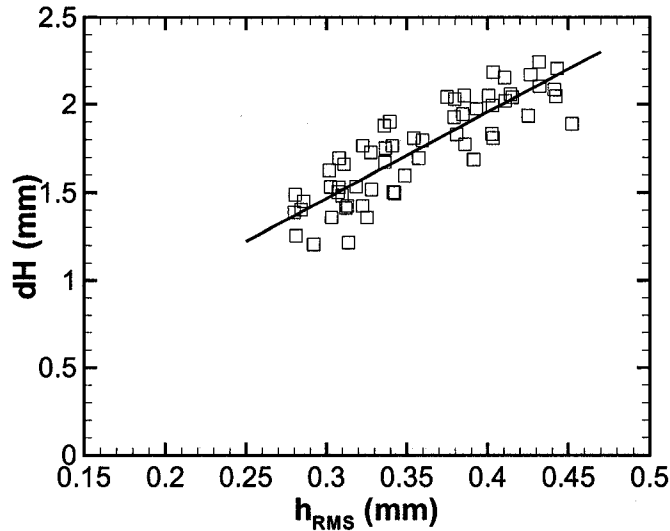


Figure 2.17: Linear relationship between mean large wave amplitude and RMS wave heights. In this case  $dH = 4.89h_{RMS}$  with  $r^2 = 0.75$ .

### 2.5.3 Pressure Drop

The two-phase pressure drop was measured over a one meter distance at a sampling rate of 1000 Hz and averaged over 15 seconds. Based on the calibration curve, the uncertainty of this measurement was taken as  $\pm 1.42$  Pa. As can be seen in Figure 2.18, the pressure drop appears to be linearly proportional to the increase in superficial gas velocity. While there is an increase in pressure drop with liquid flow rate, it is not the primary factor affecting the pressure drop.

While the pressure drop results give an indication of the losses in the system they do not distinguish between the losses caused by the wavy interface

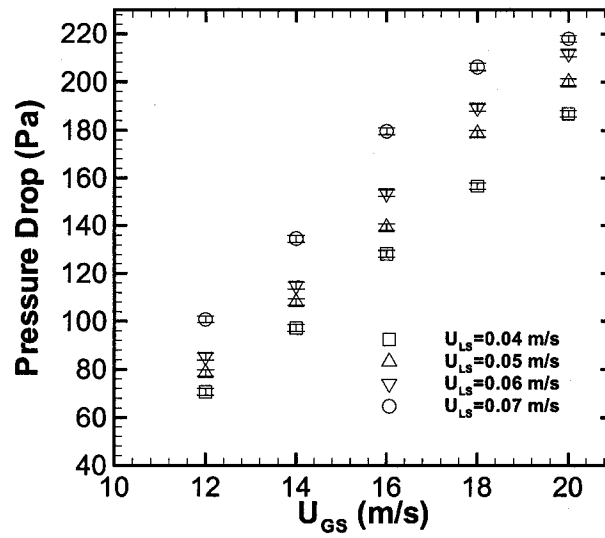


Figure 2.18: Linear relationship between pressure drop and superficial gas velocity.

and other frictional losses. In order to determine the effect of the interface on frictional losses, the interfacial friction factor,  $f_i$ , was examined and compared with the friction factor based on the assumption of a smooth interface  $f_s$ . In order to calculate these parameters, the two phase momentum equations (Taitel and Dukler, 1976) were used as described by Equation 2.9 and Equation 2.10.

$$-A_G \left( \frac{dp}{dx} \right) - \tau_{WG} P_G - \tau_i S_i = 0 \quad (2.9)$$

$$-A_L \left( \frac{dp}{dx} \right) - \tau_{WL} P_L + \tau_i S_i = 0 \quad (2.10)$$

From the experimental data, the pressure drop and respective areas were be determined while  $\tau_{WG}$  was be calculated in terms of the friction factor,  $f_G$ , from relations described by Taitel and Dukler (1976) as

$$\tau_{WG} = f_G \frac{\rho_G U_G^2}{2} \quad (2.11)$$

where  $f_G$  was calculated from the Blasius equation for friction factor in a smooth pipe shown below.

$$f_G = 0.079 \text{Re}^{-0.25} \quad (2.12)$$

Where Re was defined as

$$Re = \frac{Q_G D_h}{A_G \nu} \quad (2.13)$$

and  $D_h$  was used since the pipe was not round and defined as

$$D_h = \frac{4A_G}{P_G} \quad (2.14)$$

Both  $\tau_i$  and  $f_i$  were then calculated from Equation 2.9 and  $f_s$  was calculated using Equation 2.12.

Calculating the results showed that  $f_i/f_s$  for air flowing alone in the pipe over the range of superficial velocities was a constant 3.6. Therefore, if the interface was smooth with no wave effects,  $f_i/f_s$  would approach that value. From Figure 2.19, the effects of the large amplitude waves can be seen, as indicated by the high value of  $f_i/f_s$ . It should also be noted that there is a slight dependence on liquid flow rate. However,  $f_i/f_s$  appears to be insensitive to changes in superficial gas velocity. This is unlike previous work done by Shi and Kocamustafaogullari (1994) where a monotonic increase in  $f_i/f_s$  was seen with increasing superficial gas velocity.

Most of the results presented so far in this chapter including average film height, RMS wave heights and interfacial friction factor appeared to be insensitive to changes in gas velocity over the range tested, while the same parameters in circular pipes showed a definite dependence in superficial gas velocity ((Paras et al., 1994) and (Shi and Kocamustafaogullari, 1994)). One reason for this could be that in the experiments presented here the interface

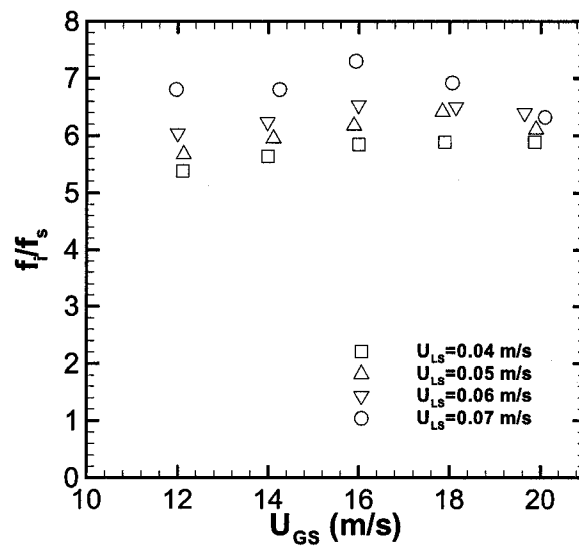


Figure 2.19: Influence of gas and liquid superficial velocities on interfacial friction factor. It can be seen that the that while the friction factor increased with increasing  $U_{LS}$ ,  $f_i/f_s$  remained constant with increasing  $U_{GS}$ .

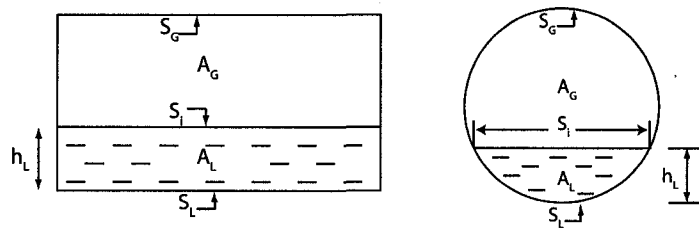


Figure 2.20: The effects of different geometry on the cross-section of the flow system

length,  $S_i$ , remained constant over the range of velocities tested. Even at the highest superficial velocities the walls of the duct were never wetted. Due to geometry and velocity profiles for circular pipes, this is not the case. Even with small changes in superficial velocity the length of the interface changes. As the gas velocity increases the changes in pressure cause the liquid to move up the sides of the pipe. The differences in geometry can be seen in Figure 2.20. In this way the effect caused by the wetting of the apparatus walls was removed enabling the isolation of the interface.

Many models have been developed to predict the interfacial shear stress in stratified gas-liquid flows (Taitel and Dukler (1976); Cheremisinoff and Davis (1979); Andritsos and Hanratty (1987a)). Due to the geometry used in this experiment and the constant interface length the models drastically under-predict the interfacial friction factor. As such the data presented here are difficult to compare with models for circular pipes.

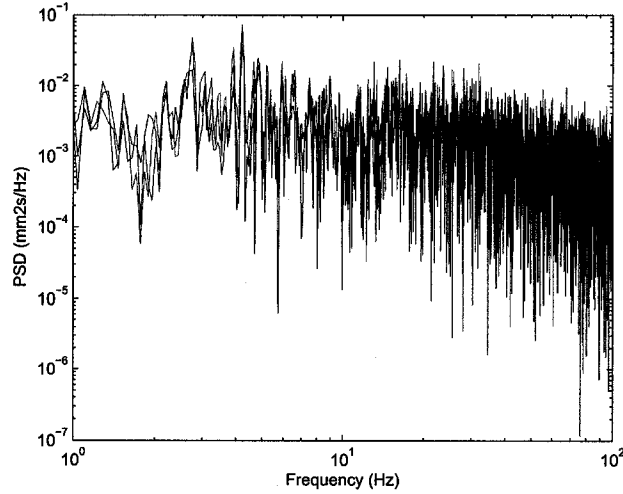


Figure 2.21: Power spectral density for the  $U_{GS} = 20\text{m/s}$  and  $U_{LS} = 0.04\text{m/s}$  condition

#### 2.5.4 Wave Frequency

The dominant wave frequency was determined by estimating the power spectral density of the wave heights using the periodogram Fourier transform techniques. The discrete Fourier of the data set was determined from:

$$X_k = \sum_{j=0}^{N-1} x_j e^{-i2\pi kj/N} \quad (k = 0, 1, 2, \dots, N) \quad (2.15)$$

From there, the power spectral density was then determined by:

$$S_k = W_s |X_k|^2 \quad (2.16)$$

where  $W_s$  is a window function, in this case a rectangular window.

From this Figure 2.21, it can be seen that the dominant frequencies at

each of the three points along the interface correspond with one another and although there is a lot of noise, the peaks are still very distinct. Plotting the dominant frequencies as a function of superficial liquid velocity is shown in Figure 2.22. It is clear that the dominant frequencies tend to lie between 3 Hz to 30 Hz. For the range of gas velocities tested, Paras et al. (1994) observed frequencies between 1 Hz and 5 Hz and Shi and Kocamustafaogullari (1994) observed frequencies between 2 Hz and 4 Hz. From Figure 2.22 it can be seen that for the lower superficial gas velocities the dominant frequencies reach a maximum at  $U_{LS}=0.05$  m/s. As superficial liquid velocity then increased to 0.07 m/s, the dominant frequencies for the lower superficial gas velocities decreased sharply and then stabilized around 5 Hz. At higher superficial gas velocities there was much less variation in dominant frequencies with superficial liquid velocity. Over the range of superficial liquid velocities tested, the dominant frequency seemed to lie between 7 Hz to 12 Hz.

Work done by Shi and Kocamustafaogullari (1994) showed that the dominant frequencies for 2-D waves are between 16 Hz to 18 Hz. As the superficial gas velocity increased a sharp decrease in dominant frequencies occurs when the waves start to transition between 2-D and large amplitude waves. Once the large amplitude waves appear the dominant frequencies appear to be stable around 2-3 Hz and then gradually increase with increasing superficial gas velocities while being fairly insensitive to changes in liquid flow rate. This behaviour was also mirrored in the results presented here. At lower superficial gas velocities there was an increase followed by sharp decrease in dominant

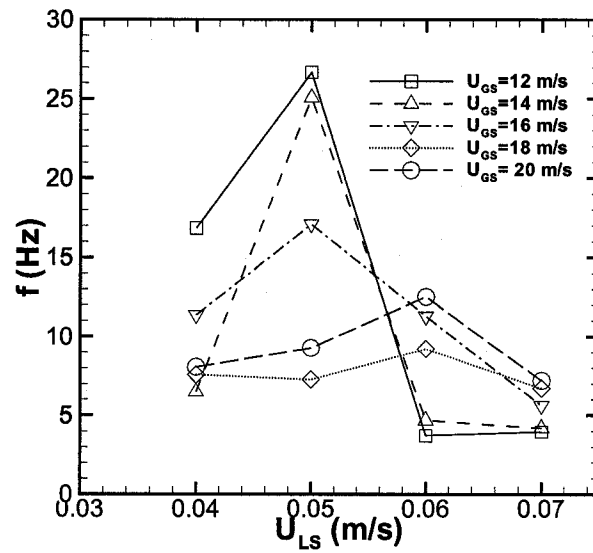


Figure 2.22: Dominant wave frequency as a function of superficial liquid velocity

frequency with increasing liquid flow rate, corresponding to the appearance of large amplitude waves. At higher gas velocities, where the waves appear to be roll waves, the dominant frequencies appeared to be insensitive to both gas and liquid superficial velocities and were stable between 7 Hz to 12 Hz.

The power spectral density of the wave heights as a function of superficial liquid velocity can be seen in Figure 2.23. The dependence on superficial liquid velocity can be clearly seen. It appears that the power increases with increasing liquid flow rate; however, there seems to be no significant dependence on the superficial gas velocity.

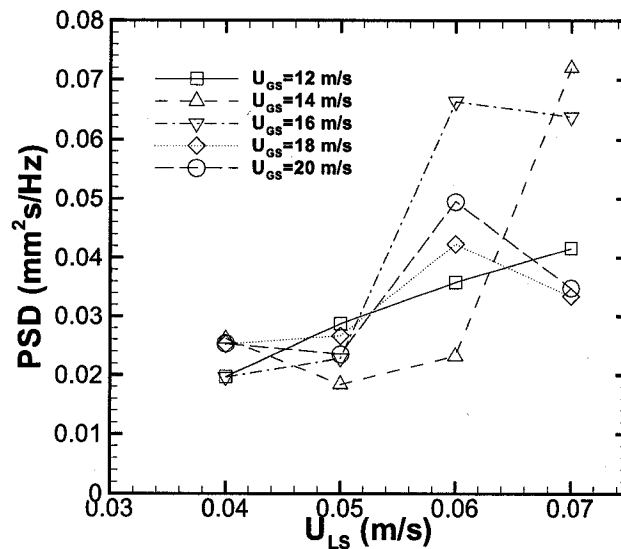


Figure 2.23: Power spectral density of the waves as a function of superficial gas velocity

## 2.6 Conclusion

The apparatus and experimental setup were designed and fabricated in order to effectively visualize the air-water interface of stratified two phase flow. The measurement method used for determining the instantaneous height of the liquid layer was developed specifically to thoroughly characterize the wavy interface. The uncertainty associated with the measurements was taken as the resolution of the instrument,  $\pm 0.08\text{mm}$ . Since the thicknesses being measured were between 0.5 mm and 3.5 mm an uncertainty of  $\pm 0.08\text{mm}$  was about 2.5% of full scale. The uncertainty in this measurement could be reduced by calibrating the system with a more proven film height measurement technique such as wire probes. Any errors caused by post processing could be reduced by the use of a more powerful laser. This would create more intense illumination allowing for the use of more polarizing filters which would remove more of the reflections thereby increasing the accuracy of the system. Using a greater magnification lens on the camera would also increase the resolution of the system. The measurement system developed is simple to set up and calibrate and is able to provide instantaneous height data over the interface cross-section. The uncertainty in the measurements is solely a function of the precision of the equipment used.

The data gathered provided information on instantaneous film heights, average film heights, RMS wave heights, mean large-wave amplitude, pressure drop and dominant frequencies for a range of superficial velocities. The in-

stantaneous time traces illustrated the shape of the waves and clearly showed the transition to large amplitude waves. The trends observed for average film height, RMS wave heights and mean large wave amplitudes were similar to results reported by previous researchers mentioned in this report. The differences in actual values could be explained by differences in size and geometry.

Pressure drop data and corresponding interfacial friction factors were also determined and while the results did not correspond with the trends seen by Shi and Kocamustafaogullari (1994), one explanation of these discrepancies could be the constant interface length in this experiment. In circular pipes the interface length changes with gas velocity which causes the liquid layer to move up the sides in the pipe. In this case even at the highest superficial velocities the liquid did not wet the sides of the apparatus keeping the interface length constant.

The dominant frequencies of the waves were consistent with the trends presented by Shi and Kocamustafaogullari (1994). At lower superficial velocities when the waves appeared to be in the midst of transitioning to roll waves the dominant frequencies were around 30 Hz. As the gas velocity increased and the waves transitioned to roll waves the dominant frequency dropped sharply and then stabilized around 7 Hz-12 Hz.

All the major characteristics of interfacial waves discussed in previous papers were observed in this experiment using the measurement method presented. In addition this method can be used to produce surface plots and characterize the interface along the cross-stream.

## BIBLIOGRAPHY

- Andritsos, N. and Hanratty, T. J. (1987a). Influence of interfacial waves in stratified gas-liquid flows. *AIChE Journal*, 33(3):444-453.
- Andritsos, N. and Hanratty, T. J. (1987b). Interfacial instabilities for horizontal gas-liquid flows in pipelines. *International Journal of Multiphase Flow*, 13(5):583-603.
- Brown, R., Andreussi, P., and Zanelli, S. (1978). The use of wire probes for the measurement of liquid film thickness in annular gas-liquid flows. *The Canadian Journal of Chemical Engineering*, 56:754-757.
- Cheremisinoff, N. P. and Davis, E. J. (1979). Stratified turbulent-turbulent gas liquid flows. *AIChE Journal*, 25:48-58.
- Fukano, T., Ishida, K., Morikawa, K., Nomura, H., Takamatsu, Y., and Sekoguchi, K. (1979). Liquid films flowing concurrently with air in a horizontal duct. *JSME*, 22:1374-1381.
- Humphreys, J. S. (1987). Improving the performance of those orifice plates. *Process Engineering*, 68(2):37-41.

- Mandhane, J. M., Gregory, G. A., and Aziz, K. (1974). A flow pattern map for gas-liquid flow in horizontal pipes. *International Journal of Multiphase Flow*, 1:537–553.
- Miya, M., Woodmansee, D. E., and Hanratty, T. J. (1971). A model for roll waves in gas-liquid flow. *Chemical Engineering Science*, 26:1915–1931.
- Mouza, A. A., Vlachos, N. A., Paras, S., and Karabelas, A. (2000). Measurement of liquid film thickness using a laser light absorption method. *Experiments in Fluids*, pages 355–359.
- Ottens, M., Hoefsloot, H., and Hamersma, P. J. (2001). Correlations predicting liquid hold-up and pressure gradient in steady-state (nearly) horizontal co-current gas-liquid pipe flow. *Chemical Engineering Research and Design*, 79:581–592.
- Ozgu, M., Chen, J., and Eberhardt, N. (1973). A capacitance method for measurement of film thickness in two-phase flow. *Review of Scientific Instruments*, 44(1):1714–1716.
- Paras, S., Vlachos, N., and Karabelas, A. (1994). Liquid layer characteristics in stratified-atomization flow. *International Journal of Multiphase Flow*, 20(5):939–956.
- Shedd, T. A. and Newell, T. A. (2004). Characteristics of the liquid film and pressure drop in horizontal, annular, two-phase flow through round, square and triangular tubes. *Journal of Fluids Engineering*, 126:807–817.

- Shi, J. and Kocamustafaogullari, G. (1994). Interfacial measurements in horizontal stratified flow patterns. *Nuclear Engineering and Design*, 149:81–96.
- Taitel, Y. and Dukler, A. E. (1976). A model for predicting flow regime transitions in horizontal and near horizontal gas-liquid flow. *AIChE Journal*, 22(1):47–55.

## CHAPTER 3

### DRAG REDUCTION

#### 3.1 Introduction

This chapter discusses the effect of drag reducing additives (DRA) on the interface of stratified two phase flow. While there has been work done in this area, much of it has concentrated on DRA's effect on annular flow (Manfield et al., 1999). The goal of this chapter was to visualize and characterize its effect on the stratified interface. Section 3.2 discusses background information on DRA, theories on how it effects the flow and previous work and their results. Section 3.3 describes the experiment and method used to obtain information on the interface. Section 3.4 presents and discusses the results of the experiment. Finally Section 3.5 summarizes and presents the conclusions of the study.

### 3.2 Background

Drag reduction can be defined as a decrease in the frictional pressure drop in a given system for a given flow rate and can be defined algebraically as:

$$DR = \frac{\Delta P - \Delta P_{DRA}}{\Delta P} = 1 - \frac{\Delta P_{DRA}}{\Delta P} \quad (3.1)$$

In this case drag reduction is achieved through the addition of a long chain, high molecular weight ( $10^6 - 10^7$  kg/kmol ) polymer. While the effects of adding a polymer to the flow have been known for a long time the mechanism responsible for the effect is still not properly understood.

Toms (1948) discovered that the addition of polymer to a single phase flow will reduce the frictional resistance at the wall. It was determined that the addition of DRA does not change the physical properties of the fluid, but instead interferes with the turbulent structure (Zohourian-Mashmoul et al., 1994). Sellin et al. (1982) proposed that the drag reduction phenomenon is related to the elasticity of the polymer molecules. The molecules extend in turbulent flow in regions of high elongational strain. This also explains why DRA has no effect in laminar flow since there are no high regions of elongational strain. Little et al. (1975) suggested that DRA molecules are active in between the viscous sublayer and the turbulent core in the centre of the pipe and work to interfere with the turbulent eddies that move through this zone and "burst" into the turbulent core. It is known now that the drag reducing abilities of the polymer are only activated once a critical level of

shear stress is attained. This causes the polymer to stretch introducing an anisotropic effect which changes the structure of the turbulence (Fore et al., 2004).

Other studies have shown that for a single phase fluid the drag reduction is achieved through a reduction in Reynolds stress and velocity fluctuation normal to the wall Warholic et al. (1999). In addition they discovered that the mean velocity profile was found not to follow the classical log law. Jovanovic et al. (2006) have suggested that the DRA suppresses the viscous diffusion at the wall which in turn causes a decrease in the turbulence production. According to these researchers, the polymer starts as rolled up chains and exposure to turbulence causes the polymer to partially unroll and stretch in the mean flow direction. In this state the polymer essentially controls the size of the characteristic small scales in the flow. They hypothesized that the mechanism of drag reduction is related to the ability of the polymer to resize the turbulent small scales.

Recently Vlachogiannis et al. (2003) and Liberatore et al. (2004) carried out studies to determine the effect of molecular size of the polymer on its ability to realize a drag reduction in a flow. It was determined that molecular aggregation has a large effect on the ability to produce a drag reduction and may be more important than the polymer's molecular weight in determining its effect.

Most studies regarding drag reduction involve homogeneous polymer solutions in fully developed turbulent channel flow. This is usually accomplished

in one of two ways. Either a polymer solution is mixed in advance and used in the channel or a high concentration master solution is mixed and then injected into the flow in such a way that it produces a homogenous solution at a desired concentration (Fore et al., 2004).

Although much work has been done on drag reduction in multiphase flow only a few studies have been done in the horizontal wavy stratified regime. One of the first studies done with DRA in multiphase flow was done in the annular mist regime by Sylvester and Brill (1976). These experiments were done in a horizontal, 1.27 cm diameter pipe 6.1 meters in length. 100 ppm of Polyethylene oxide was added to the flow resulting in up to a 37% reduction in pressure drop. However no explanations were given for the results.

Al-Sarkhi and Hanratty (2001a) discussed the influence of Percol 727 on horizontal annular air-water flow in a 0.0953 m diameter pipe. Drag reduction increased with increasing polymer concentration up to 15ppm resulting in a drag reduction of 48%. At this maximum drag reduction the friction factor was close to that of gas flowing alone ( $f/f_G \approx 1$ ). At large drag reductions the annular flow regime was changed to a stratified pattern. They suggested that the addition of the polymer destroyed the disturbance waves that were causing the drop formation.

It was also discovered that the results obtained were dependent on the method of mixing the polymer. Al-Sarkhi and Hanratty (2001a) used a master solution that was injected, without using a pump, into the flow. The amount of solution was measured out by a rotameter in order to achieve the

desired concentration. They determined that a master solution of 1000 ppm generated the largest drag reduction. Previously Warholic et al. (1999) theorized that having a master solution caused larger entanglements of polymer chains resulting in greater drag reductions.

Al-Sarkhi and Hanratty (2001a) found that drag reduction was also dependent on the mode of polymer introduction. They experimented with injecting the polymer solution at different points along the apparatus. One set of tests was performed having the polymer solution injected into the liquid before the air and liquid phases were mixed and the other set of tests had the polymer injected directly into flow once the annular pattern was already developed. Direct injection was more effective, greatly increasing the drag reduction especially at lower DRA concentrations.

In another study Al-Sarkhi and Hanratty (2001b) investigated the addition of Percol 727 on annular air-water flow in a 0.0254 m diameter pipe. For the smaller pipe diameter, the maximum drag reduction achieved was 63% but required polymer concentrations of 30 ppm. They observed that drag reduction increased with increasing liquid flow rate and decreased for increasing air flow rate. Again at large drag reductions the annular flow regime was suppressed to a stratified flow regime.

Al-Sarkhi and Soleimani (2004) studied the effect of DRA on the two-phase horizontal flow patterns in a 0.0254 m diameter pipe. With the addition of DRA, the annular pattern (at lower gas velocities) was transformed to stratified and at higher gas velocities changed to stratified-annular. Their

experiments correlated with the results of Al-Sarkhi and Hanratty (2001b), indicating that the effect of DRA is greater at lower gas velocities.

Baik and Hanratty (2003) studied the effects of the polymer on stratified flow in a large diameter pipe. For the 9.53 cm diameter pipe at the superficial velocities tested, they hypothesized that the addition of DRA to the flow both damped the interfacial waves and reduced the turbulence in the liquid.

### 3.3 Experimental Setup and Method

All the experiments were conducted in the apparatus described in Chapter 2. Briefly, a transparent rectangular pipe of cross-section 50.8 mm by 25.4 mm and 2.5 m in length was used for all tests. Compressed air entered through two air hoses at one end of the apparatus. An orifice plate was used to measure the inlet air flow rate, and necessary adjustments to the flow rate were made using valves connected to the air supply line. The polymer solution was mixed in a 0.34 m<sup>3</sup> tank and was pumped through the system using a moving vane positive displacement pump. The liquid entered through two hoses through the bottom of the apparatus, 18 diameters downstream from the air inlet. A rotameter was used to measure the liquid flow rate at the liquid inlet and all necessary adjustments to the flow rate were made by adjusting the pump speed. The two streams were separated by a thin metal plate (0.8mm thick) for 45 diameters before mixing. At the end of the apparatus The two fluid streams exited into the separator. Since the inlet of the separator was larger than the cross section of the apparatus, the system

was open to the atmosphere and negligible back pressure was imposed. In order to prevent degradation of the polymer the liquid had only one pass through the apparatus, after which it was disposed. The apparatus and all its components are described in detail in Chapter 2, Section 2.3.

A variable capacitance diaphragm pressure transducer was used to measure the two phase pressure drop over a one meter distance. The interface measurements were taken one meter downstream of the mixing point over the cross section of the duct. This was done using the laser induced fluorescence and video camera setup and method described in Chapter 2 section 2.3 and section 2.4.

Tests were conducted in the wavy stratified regime. For this setup this consisted of superficial air velocities ranging from 12 m/s to 20 m/s and superficial liquid velocities from 0.04 m/s to 0.07 m/s. Air flow rates and pressure drop data were recorded by a data acquisition system at a sampling frequency of 1000 Hz for 15 seconds. The interface measurements were recorded by the video camera at 1000 frames/second over 2.5 seconds. A 100 Hz Equiripple low pass filter was applied to the data to remove the high frequency noise. The specifications of the filter can be seen in Appendix B.

At the beginning of every run, the air was switched on first and set to the designated value. After the air reached steady state the liquid flow was initiated and the pump was adjusted to give the desired flow rate. The tests were performed for DRA concentrations of 5 ppm, 10 ppm, 20 ppm, 30 ppm, 40 ppm and 50 ppm. These were compared with the no DRA case in order

to determine the effects of the various concentrations of the additive on the system. A solution of a co-polymer of polyacrylamide and sodium-acrylate (Percol 727) in water was used. The polymer was provided by Ciba Chemicals by the commercial name of Magnafloc 1011.

The solution at the required concentration, was mixed in a tank rather than having a master solution injected directly into the flow. The polymer was in powder form and was mixed in solution following the instructions by Foshee et al. (1976). An agitator was attached to the tank and set to mix at 75 rpm in order to avoid degradation of the polymer. The polymer was sprinkled over 60 seconds into the vortex caused by the agitator. The stirrer then mixed the solution for 2 to 3 hours. The solution was allowed to stand overnight and then stirred again about 20 minutes before using.

Since the concentrations normally used to reduce drag in pipe flow are quite low (0-100ppm) the density of the solution was approximated by the density of the liquid at its temperature and atmospheric pressure. However the viscosity drastically changes when the polymer is added to the flow. The addition of the polymer to water transforms it into a non-newtonian fluid where the viscosity decreases with shear rate.

## 3.4 Experimental Results

### 3.4.1 Introduction

The results of the experiments performed in the air-water-polymer system are presented in this section. Discussion of pressure drop and interface characteristics including film thickness traces, RMS wave heights, wave amplitudes and pressure drop for various concentrations of DRA are included in this section. Comparisons with the results from Chapter 2 and previous studies by other researchers are also presented.

### 3.4.2 Effect of DRA on Interfacial Waves and Flow Regime

In order to determine the effect of DRA on the interfacial waves, the film height was measured at three points across the a 7mm distance in the centre of the duct. This was done for each pair of gas and liquid flow rates and at all tested concentrations of DRA.

As mentioned in section 3.2, the addition of DRA to a two phase flow can cause a flow regime change. However, without DRA, at all test conditions the flow regime remained in the stratified area so the addition of DRA did not cause a regime change. Instead a change in wave structure was observed. Without DRA present and at low superficial gas velocities, the waves appeared in a transitional regime, not yet large amplitude waves. As the gas superficial velocity increased, the waves quickly entered into the large amplitude wave regime. With the addition of DRA, suppression of the large

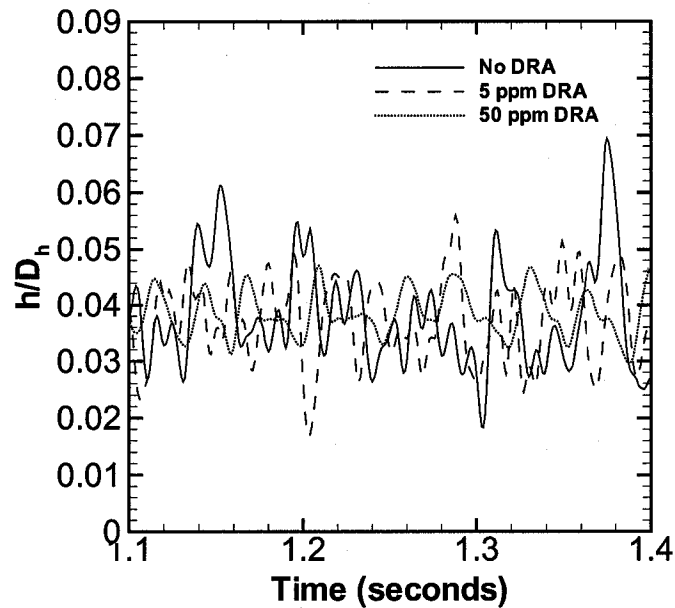


Figure 3.1: Comparison of dimensionless instantaneous film height for  $U_{GS} = 12\text{m/s}$  and  $U_{LS} = 0.04\text{m/s}$  of various concentrations of DRA. Even at a concentration of 5 ppm the reduction in amplitude is apparent.

amplitude waves and transition waves occurred depending on the concentration of DRA added and the respective flow rates. These reductions in wave amplitudes occurred even at a low concentration of 5ppm DRA. This can be seen in Figure 3.1.

The change in the structure of the waves with the addition of various concentrations of DRA can be seen in Figure 3.2. In this figure the surface waves of a flow with a superficial gas velocity of 16 m/s and a superficial liquid velocity of 0.05 m/s was studied. In the case with no DRA, the waves are large amplitude waves as can be seen by the steep front face and shallower

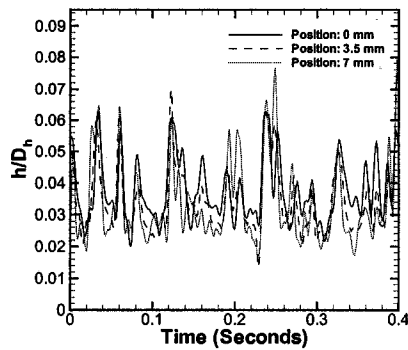
rear face. There is also some variation across the 7mm cross-stream distance. Even with the addition of 5ppm DRA there is a definite decrease in wave amplitude, although the waves still have a somewhat irregular appearance. With the addition of 10 ppm DRA the wave amplitude decreased further and they have taken on a more regular appearance. The addition of 20 ppm DRA or more caused the large amplitude waves to be suppressed and take on a more regular appearance such that they resembled 2-D waves. At this point there is no real variation in the waves across the 7mm cross-stream distance. As the superficial velocities increased, the ability of a given concentration to suppress large amplitude waves from forming decreased. The effect of DRA on the structure of the waves was highly dependent on the flow conditions.

### 3.4.3 Effect on Average Film Thickness

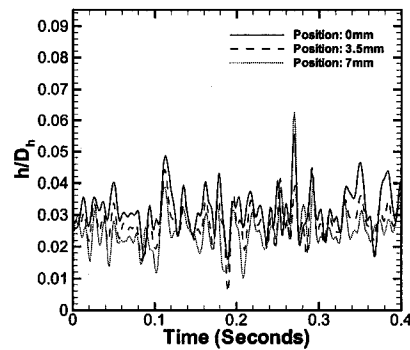
The addition of DRA to the liquid did not appear to have a significant effect on average liquid height. Figure 3.3 shows the average dimensionless liquid height ( $\bar{h}/D_h$ ) as a function of DRA concentration for a superficial liquid velocity of 0.05 m/s. It can be seen that there is a slight change in the average height with the addition of DRA but is not necessarily correlated with the concentration of the polymer. It is curious to note that the average height results for 10ppm concentration across all superficial gas and liquid velocities are significantly lower than all the other cases presented. No reasonable explanation for this behaviour was discovered. If this discrepancy is disregarded for a moment it can be determined that the maximum difference

in average height of films with no DRA as compared to films with DRA was less than 15%.

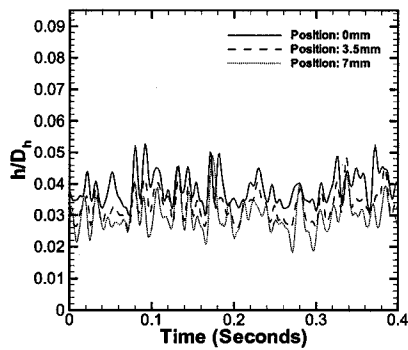
The addition of DRA did not effect the influence of gas and liquid super-



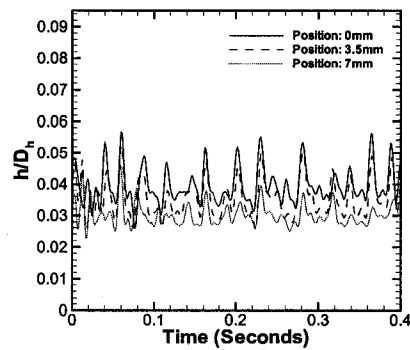
(a) no DRA.



(b) 10 ppm DRA.



(c) 30 ppm DRA.



(d) 50 ppm DRA.

Figure 3.2: Comparison of waves for  $U_{GS} = 16m/s$  and  $U_{LS} = 0.05m/s$  for various concentrations of DRA. The waves with no DRA added resemble large amplitude waves. With the addition of 10ppm the waves have decreased in amplitude and have taken on a more regular occurrence. With the addition of 20ppm of DRA or more the wave amplitudes are further suppressed, they have a significantly more regular appearance and there is little variation in the cross-stream direction.

ficial velocities on the average film height. No matter the concentration of the polymer, an increase of gas flow rate caused a sharp decrease in average film height while an increase in liquid flow rate caused a moderate increase in the average film height. Figure 3.3 shows the decrease in average film height with increasing superficial gas velocity for all concentrations of DRA tested.

Figure 3.4 shows dimensionless average height as a function of superficial liquid velocity. It also compares flow conditions with no DRA to the same flow conditions at the concentration of DRA that produced maximum drag reduction. From this it can be seen that even with the addition of DRA that produces maximum drag reduction there was very little change in the average liquid height. The difference increased with increasing gas superficial velocity. At 20 m/s the addition of DRA caused a decrease in average height of approximately 10%. One possible explanation for the lack of effect is that there was no change in the length of the interface since no wetting of the duct walls occurred. Another explanation is the lack of droplet entrainment. Even at the highest superficial gas velocity hardly any droplet entrainment occurred; therefore, the only effect of the DRA on the film thickness was the dampening of the waves which caused a slight decrease in average film height.

#### 3.4.4 RMS Wave Heights

Another method of determining the effect of DRA on the interface is to compare RMS wave heights,  $h_{RMS}$ , of different concentrations of DRA. This

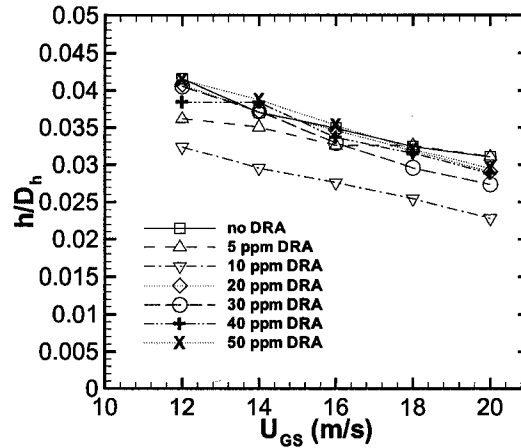


Figure 3.3: Comparison of dimensionless instantaneous film height for various concentrations of DRA and  $U_{LS} = 0.05 \text{ m/s}$ . No significant difference in heights with the addition of DRA.

parameter can be used to characterize the nature of the waves and is defined as follows:

$$h_{RMS} = \sqrt{\frac{1}{n} \sum_{i=1}^n h_i^2} \quad (3.2)$$

It can be seen in Figure 3.5 that the addition of DRA caused a reduction in  $h_{RMS}$  values, however; it can also be seen that concentrations above 10 ppm did not seem to produce any significantly greater reductions. Maximum reduction in RMS wave heights occurred around 30 ppm for superficial liquid velocities of 0.04 m/s and 0.05 m/s over the total range of superficial gas velocities. For superficial liquid velocities of 0.06 m/s and 0.07 m/s maximum reduction of RMS wave heights occurred at a concentration of 50 ppm.

The RMS values appeared to be slightly dependent on superficial gas

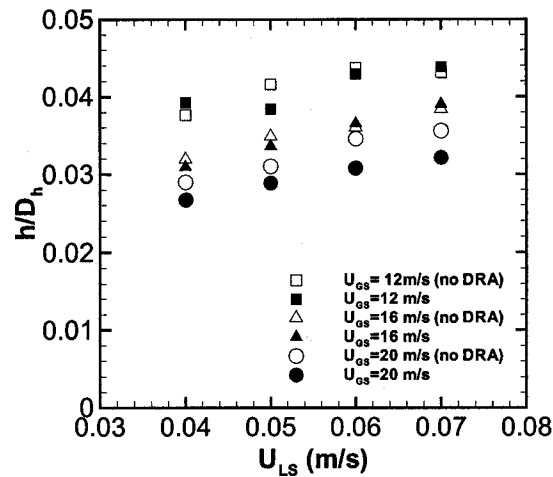


Figure 3.4: Comparison of dimensionless average film height between flow conditions with no DRA and flow conditions at the concentration of DRA that produced maximum drag reduction. It can be noticed that even at maximum drag reduction the addition of the polymer has very little effect on the average liquid film height.

velocity, decreasing as the velocity increased. The addition of the polymer did not alter this trend as it has been observed in stratified flow with no polymer additive. The observation of increasing RMS values with increasing superficial liquid velocity that was observed in the flow cases without DRA was also noted in these experiments as can be seen in Figure 3.6.

In addition to the effect of DRA on wave structure and RMS values it also had an effect on the mean large wave amplitude,  $dH$ . This parameter was determined as the largest difference between crest and trough over a 200 millisecond time section for a given cross-stream location. This data was taken over the 2.5 seconds and the values were then averaged to give the

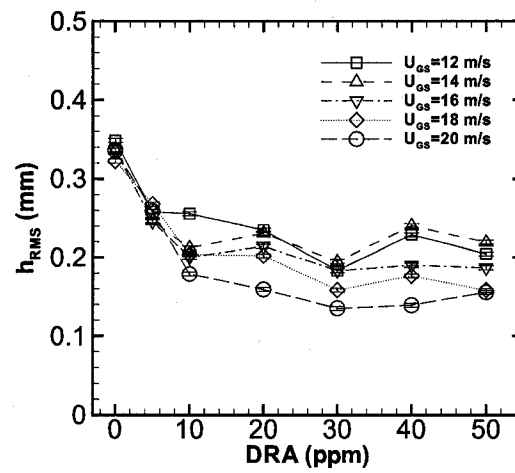


Figure 3.5: Comparison of  $h_{RMS}$  for various concentrations of DRA at  $U_{LS} = 0.05m/s$ . A significant drop in  $h_{RMS}$  values can be seen with the addition of DRA up to a concentration of 10ppm. With concentrations above 10ppm no greater reduction is observed.

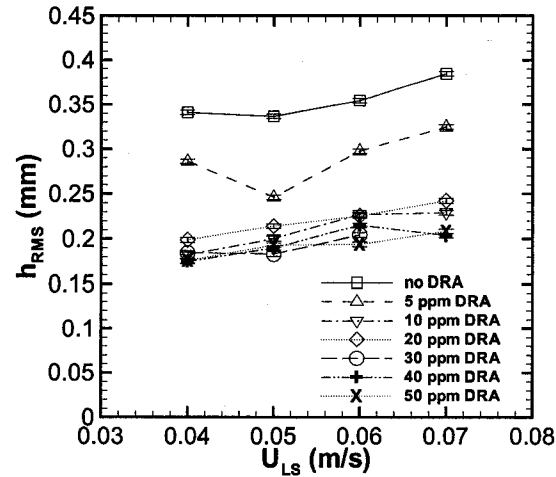


Figure 3.6: Comparison of  $h_{RMS}$  with  $U_{LS}$  for various concentrations of DRA at  $U_{GS} = 16m/s$ . Even with the significant amount of uncertainty the trend of increasing values of  $h_{RMS}$  with increasing  $U_{LS}$  is observed.

result.

The mean large wave amplitude as a function of DRA concentration can be seen in Figure 3.7. From this figure it can be observed that the addition of DRA caused a decrease in the mean large wave amplitude. The decrease in mean large wave amplitude values occurred with the increasing concentration of DRA up to a concentration of about 30 ppm and then stabilized around those values even with the addition of more DRA. This leveling off effect also corresponded with the leveling off effect observed in the RMS wave heights. These results correspond with the changes in wave type caused by the polymer discussed in Section 3.4.2. As the large amplitude waves were suppressed the mean large wave amplitude naturally decreased.

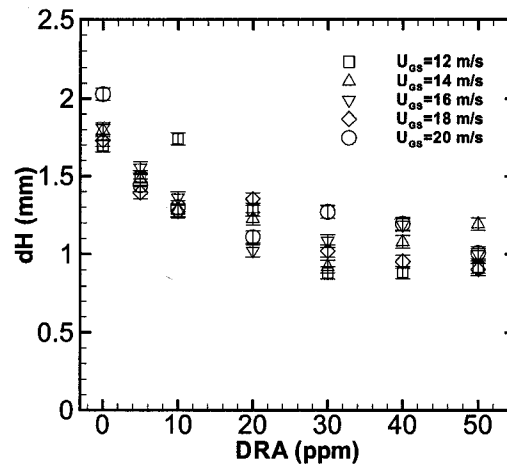


Figure 3.7: Comparison of  $dH$  with concentration for  $U_{LS}=0.06$  m/s.  $dH$  decreases with increasing DRA concentration up to 30 ppm. The values of  $dH$  stabilize with any increase in concentration above 30 ppm.

The mean large wave amplitude can also be related to RMS wave heights. As can be seen in figure 3.8, the relationship is a linear one. For stratified flow in circular pipes it has been found that  $dH = 2\sqrt{2}h_{RMS}$  accurately describes the relationship (Paras et al., 1994). For the experimental setup used here it was found for a flow with out the addition of DRA that  $dH = 4.89h_{RMS}$  described the relationship between the RMS values and the large wave structures. With the addition of DRA the relationship remains linear only with a steeper slope. The slope of the line was essentially the same for all concentrations of DRA used varying only between  $dH = 5.5h_{RMS}$  to  $dH = 5.7h_{RMS}$ . This variation was within the uncertainty of the measurements.

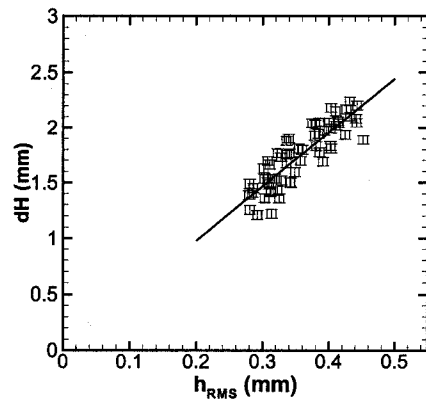
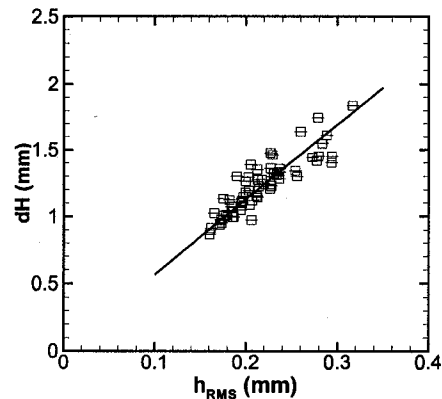
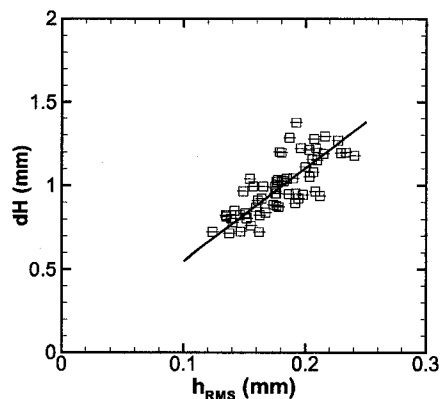
(a) no DRA where  $dH = 4.89h_{RMS}$ .(b) 10 ppm DRA where  $dH = 5.6h_{RMS}$ .(c) 40 ppm DRA where  $dH = 5.5h_{RMS}$ .

Figure 3.8: Difference in linear relationship of large wave amplitude as a function of RMS values of film thickness for various concentrations of DRA.

### 3.4.5 Drag Reduction

The drag reduction realized by the addition of a polymer to the flow can be characterized in a number of ways. One way of defining drag reduction is

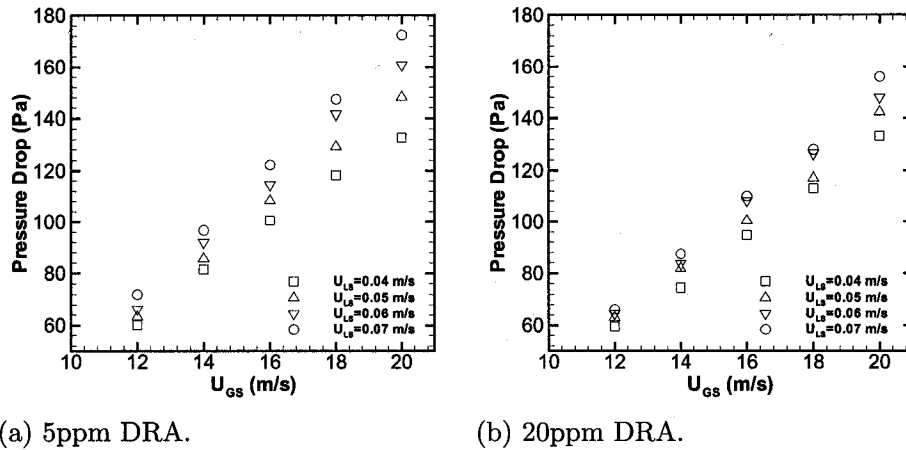
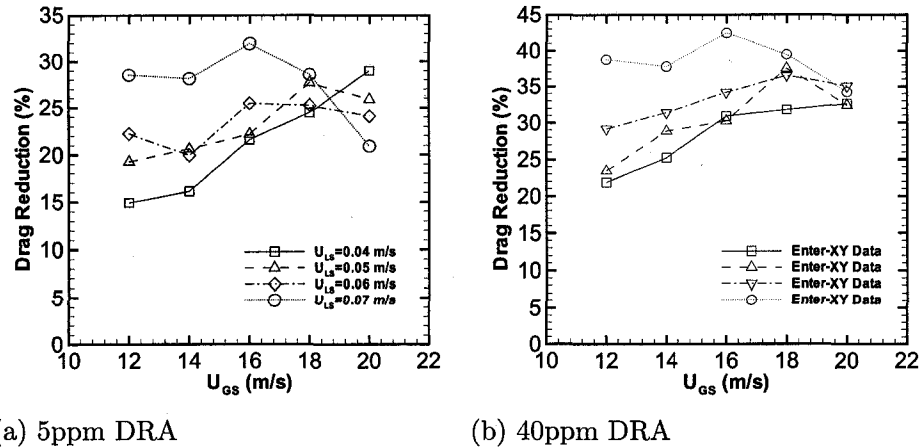


Figure 3.9: Pressure drop of the system for different liquid flow rates. Linear relationship between pressure drop and  $U_{GS}$  remains constant even with the addition of DRA.

by comparing the difference in pressure drop of the system with and without DRA as described by equation 3.1.

The pressure drop was measured over a one meter distance down the centreline of the duct. Measurements were taken at a sampling rate of 1000 Hz over a total sampling time of 15 seconds. Based on the calibration curve for the instrument the uncertainty in the measurement was taken as  $\pm 1.42$  Pa. As discussed in Chapter 2, the pressure drop appears to be a linear function of superficial gas velocity and it also increases with increasing superficial liquid velocity. These relationships did not change with the addition of DRA into the flow as can be seen in Figure 3.9.

Using the pressure drop information and equation 3.1, the percentage drag reduction for each concentration of DRA at the given gas and liquid



(a) 5ppm DRA

(b) 40ppm DRA

Figure 3.10: Effect of DRA as a function of superficial gas velocity. It can be seen that the drag reduction increases with increasing gas velocity up to around 18 m/s before decreasing slightly.

flow rates were calculated. Drag reduction of at least 15% was observed even at a concentration of only 5ppm. It was observed that drag reduction then increased with increasing concentrations up to a concentration of between 30 ppm and 40 ppm before leveling off in the same way as was observed for the mean large wave amplitude results and the RMS wave height results. This can be seen in figure 3.10. As the liquid flow rate increased an increase in drag reduction in the results was observed. An increase in superficial gas velocity up to 18 m/s also caused a drag reduction increase, however; at velocities greater than 18 m/s a decrease in drag reduction was observed.

Baik and Hanratty (2003) observed a similar trend of increasing drag reduction with increasing superficial velocities. Other work including Al-Sarkhi and Soleimani (2004), Al-Sarkhi and Hanratty (2001a) and Fernandes et al.

(2004) show greater effectiveness of DRA at lower superficial gas velocities instead. The difference in these results can be explained the by the difference in the original flow regime. Al-Sarkhi and Soleimani (2004), Al-Sarkhi and Hanratty (2001a) and Fernandes et al. (2004) all performed experiments in the horizontal annular flow regime. They noted that the addition of DRA at low superficial gas velocities caused the flow to revert to the stratified flow regime causing a large decrease in pressure drop. At the higher superficial gas velocities, even with the addition of DRA, the flow remained in the annular regime causing a less dramatic drag reduction. The behaviour of the results presented here can be explained in the same way. The suppression of roll waves caused a large reduction in pressured drop. At higher gas velocities even with the addition of DRA the wave amplitude is still significant enough that the drag reduction is less.

It was also determined that maximum drag reduction occurred at concentrations between 30 ppm DRA and 40 ppm DRA depending on the gas and liquid flow rates. At concentrations higher than those mentioned, the drag reduction did not increase but remained fairly constant at the maximum level. This behaviour has been seen in previous work including Al-Sarkhi and Hanratty (2001a), Al-Sarkhi and Hanratty (2001b) and Al-Sarkhi and Soleimani (2004). For those cases maximum drag reduction occurred at 10-15 ppm and 20-50 ppm depending on gas and liquid flow rates. The difference in results might be due to difference in pipe diameter and geometry of the apparatus.

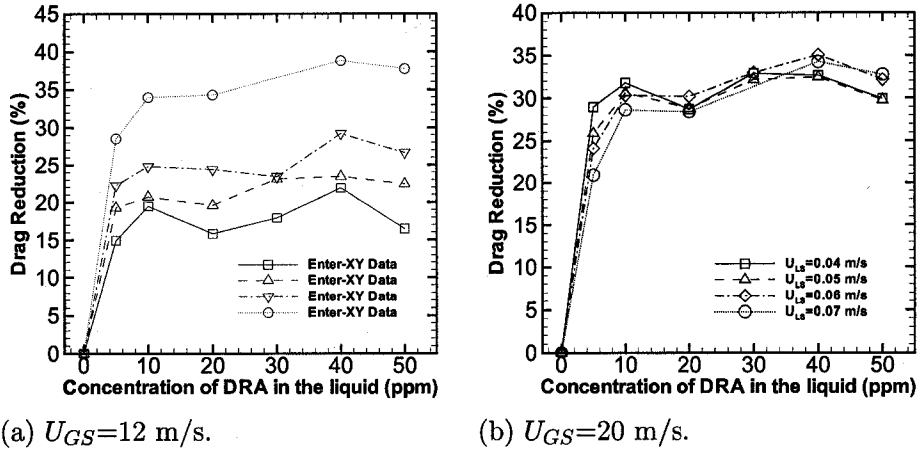
(a)  $U_{GS}=12$  m/s.(b)  $U_{GS}=20$  m/s.

Figure 3.11: Effectiveness of DRA in the liquid at the minimum and maximum superficial gas velocities tested. It can be seen that the effectiveness of a given concentration of DRA increases with increases in  $U_{LS}$ .

From Figure 3.11 it can be seen that maximum drag reduction for these flow cases is 40 ppm. It should also be noted that as the superficial gas velocity increases the influence of liquid flow rate on drag reduction is reduced. At a superficial gas velocity of 12 m/s the difference in drag reduction between superficial liquid flows rate of 0.04 m/s and 0.07 m/s was about 50%. This difference dropped to a less than 25% at a superficial velocity of 20 m/s.

The effect of drag reduction by adding a polymer to a stratified-annular flow has also been interpreted by the use of the friction factor by Al-Sarkhi and Hanratty (2001a), Al-Sarkhi and Hanratty (2001b) and Fernandes et al. (2004). They used the friction factor defined by:

$$f = \frac{D}{2\rho_G U_{GS}^2} \frac{dP}{dx} \quad (3.3)$$

and compared it with the friction factor for a pipe with smooth walls as defined by the Blasius equation.

$$f_s = 0.079Re^{-0.25} \quad (3.4)$$

Using the ratio  $f/f_s$  for flows with and without DRA gave an indication of the effect of the polymer on the flow. The values of  $f/f_s$  were also used to determine a Nikuradse sand roughness for each flow condition.

Since the flow regime for the experiments documented here, started and remained in the stratified regime the interfacial friction factor was used to further characterize the effect of DRA. By looking at the interfacial friction factor, instead of the overall friction factor in the pipe, the effects of DRA on losses at the interface could be studied. In order to determine the interfacial friction factor, the two phase momentum equation for the gas phase was used as shown below.

$$-A_G \left( \frac{dp}{dx} \right) - \tau_{WG}P_G - \tau_i S_i = 0 \quad (3.5)$$

$$-A_L \left( \frac{dp}{dx} \right) - \tau_{WL}P_L + \tau_i S_i = 0 \quad (3.6)$$

Equation 3.5 describes the balance between the pressure forces on the gas and the resisting stresses at the wall and the gas-liquid interface. Equation 3.6 describes the balance between pressure forces caused by the drag

induced on the liquid phase by the gas phase and the resisting stresses at the solid-liquid boundary.

The gas shear stress,  $\tau_{WG}$  was calculated by using the relationship given by

$$\tau_{WG} = f_G \frac{\rho_G U_G^2}{2} \quad (3.7)$$

where  $f_G$  is the fanning friction factor and was calculated by using the Blasius equation for a pipe with smooth walls (Equation 3.4). The Reynolds number was calculated using the actual gas velocity and the diameter was defined by the hydraulic diameter of the gas phase.

$$Re = \frac{\rho_G D_h U_G}{\mu_G} \quad (3.8)$$

$$D_h = \frac{4A_G}{P_G} \quad (3.9)$$

Using these equations,  $\tau_i$  was calculated from Equation 3.5.  $\tau_i$  can also be defined by the following equation :

$$\tau_i = f_i \frac{\rho_G U_G^2}{2} \quad (3.10)$$

$f_i$  was then calculated using Equation 3.10.

Comparing the interfacial friction factor with the friction factor assuming a smooth interface gave information about the nature of the roughness of the interface. These values were then compared with values calculated for various

concentrations of DRA in order to determine the effect of the polymer on the roughness of the interface.

The  $f_i/f_s$  for gas flowing alone in the pipe was constant around 3.6. A full summary of the results can be seen in Table 3.1.

Table 3.1: A summary of the  $f_i/f_s$  results for all flow conditions

$U_{Ls}$ (m/s)	$U_{Gs}$ (m/s)	No DRA	5 ppm DRA	10 ppm DRA	20 ppm DRA	30 ppm DRA	40 ppm DRA	50 ppm DRA
0.04	12	5.4	4.8	4.8	4.9	4.8	4.7	4.8
0.04	14	5.6	5.1	4.9	4.9	4.7	4.7	4.8
0.04	16	5.8	5.0	4.9	4.9	4.7	4.7	4.8
0.04	18	5.9	4.8	4.8	4.8	4.7	4.6	4.8
0.04	20	5.9	4.8	4.7	4.7	4.6	4.5	4.7
0.05	12	5.7	5.1	5.0	5.0	4.9	4.8	4.9
0.05	14	5.9	5.1	5.1	5.1	4.9	4.8	5.0
0.05	16	6.2	5.2	5.1	5.1	4.9	4.8	5.0
0.05	18	6.4	5.1	5.0	4.9	4.9	4.7	4.9
0.05	20	6.1	5.0	4.9	4.9	4.8	4.8	4.8
0.06	12	6.0	5.2	5.1	5.1	5.0	4.8	5.0
0.06	14	6.2	5.3	5.2	5.2	5.0	4.9	5.1
0.06	16	6.5	5.4	5.2	5.2	5.0	4.9	5.1
0.06	18	6.5	5.3	5.2	5.1	5.0	4.9	5.0
0.06	20	6.4	5.2	5.1	5.0	4.9	4.8	4.9
0.07	12	6.8	5.3	5.2	5.2	N/A	4.9	5.0
0.07	14	6.8	5.5	5.3	5.3	N/A	5.0	5.1
0.07	16	7.3	5.5	5.3	5.3	N/A	5.0	5.2
0.07	18	6.9	5.5	5.3	5.2	N/A	5.0	5.1
0.07	20	6.3	5.5	5.2	5.1	N/A	4.9	5.0

The closest value of  $f_i/f_s$  for the two phase conditions to the value of  $f_i/f_s$  for air only flowing in a pipe was for a concentration of 40 ppm DRA at a superficial gas velocity of 20 m/s and a superficial liquid velocity of 0.04 m/s. While this value was the closest to the value recorded to the air only case, it did not signify the largest reduction in interfacial frictional losses. This was calculated as the largest difference between  $f_i/f_s$  with and without DRA and occurred at a concentration of 40 ppm at a superficial gas velocity of 16 m/s and a superficial liquid velocity of 0.07 m/s. This flow condition and concentration of DRA is the same condition for which the maximum drag reduction of 42% calculated by Equation 3.1 was observed. However, unlike the results obtained with Equation 3.1 the maximum reductions were realized at 40 ppm for all flow conditions.

Figure 3.12 shows very clearly the effect of DRA on the interfacial frictional losses. It can be seen that the maximum reduction of  $f_i/f_s$  was achieved at a concentration of 40 ppm DRA. However it can also be seen that a significantly large reduction is accomplished with a concentration of only 10 ppm DRA. The difference in the reduction of the interfacial frictional losses between 10ppm and 40ppm was less than 10%.

Figure 3.13 shows that while the friction factor for the situation with no DRA increases with increasing superficial gas velocity, the addition of DRA to the fluid causes the friction factor to remain fairly constant over the range of superficial gas velocities. Again it can be seen that the lowest values of  $f_i/f_s$  occur for concentrations of 40 ppm.

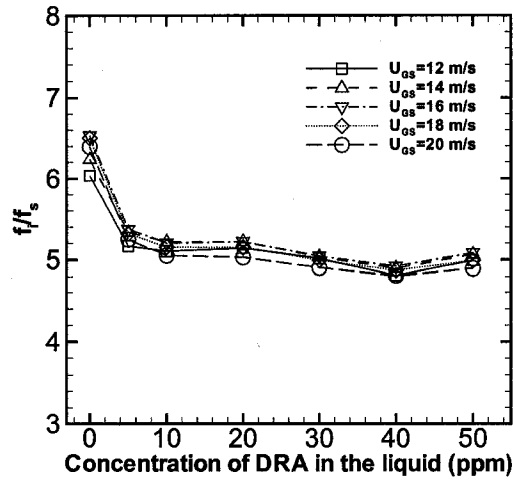


Figure 3.12:  $f_i/f_s$  as a function of DRA concentration for  $U_{LS}=0.06$  m/s. A large reduction is achieved with the addition of 5ppm DRA, but maximum reduction occurs at 40 ppm DRA.

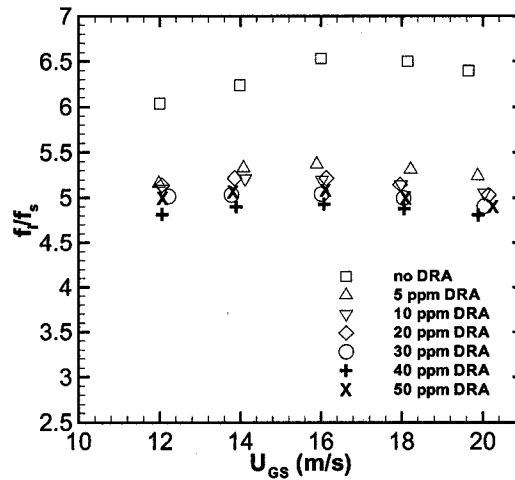


Figure 3.13:  $f_i/f_s$  as a function of  $U_{GS}$  for  $U_{LS}=0.06$  m/s. It can be observed that the addition of DRA renders the friction factor basically insensitive to changes in  $U_{GS}$ .

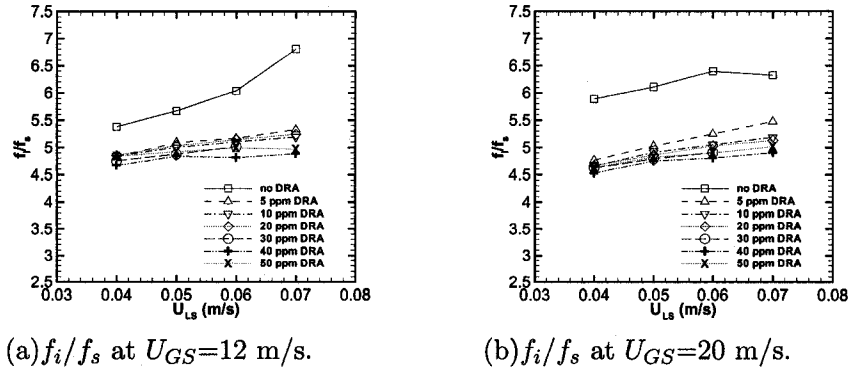


Figure 3.14:  $f_i/f_s$  as a function of  $U_{LS}$  for all concentrations of DRA. Maximum reduction in value occurs at a concentration of 40 ppm.

From Figure 3.14 it can be seen that with no DRA the friction factor increases sharply with increasing superficial liquid velocity. The addition of DRA reduces the impact of liquid flow rate and while the friction factor is still dependent on superficial liquid velocity it is not the major factor influencing the friction factor.

The ability of the polymer to affect drag reduction on the flow can be seen more clearly through the usage of  $f_i/f_s$  than through the drag reduction Equation 3.1. In addition the results of both analyses are very similar indicating that the majority of the drag reduction occurs at the gas-liquid interface.

### 3.5 Conclusion

Introducing a polymer into the two phase stratified flow had significant affects on the interfacial waves, RMS wave heights, mean large wave ampli-

tudes, pressure drop and friction factor as were discussed here. For flow conditions that created large amplitude waves, the addition of DRA caused a suppression of wave amplitude and a change to a more regular appearance.

Suppression of wave amplitude was quantified using the mean large wave amplitude which was found to decrease with increasing concentrations of DRA up to a concentration of about 30 ppm. The addition of more DRA at that point caused no significant difference. While minimum values of the mean large wave amplitude were observed at 30 ppm there was no significant drop in values between 10 ppm and 30 ppm DRA.

Average film heights were also explored and it was determined that the addition of DRA caused no significant difference especially at low superficial velocities. At higher superficial velocities there was a slight decrease in average film height which could be explained by the suppression of large waves.

Exploring the RMS wave heights, it was discovered that there was a sharp decrease in values with the addition of 10 ppm DRA. However the maximum decrease occurred between 30 ppm to 50 ppm DRA. There was also a leveling off effect that occurred around 30 ppm DRA. At higher concentrations no significant difference was noted. This effect was also noted in mean large wave amplitudes and RMS wave height results.

Drag reduction of at least 15% was obtained with a concentration of only 5 ppm. Maximum drag reduction of 42% was achieved at a concentration of 40 ppm DRA. Drag reduction increased with increasing gas superficial velocity

at low superficial liquid velocities. At higher superficial liquid velocities a decrease in drag reduction occurred starting at 18 m/s. One explanation for this behavior is that at higher superficial velocities for a given concentration of DRA, the wave amplitudes are not as significantly suppressed and as such there is less of a drag reduction.

While the maximum drag reduction was achieved at 40 ppm DRA for the conditions at which that drag reduction was realized, there was only a 10% difference in drag reduction between 10 ppm and 40 ppm. Similar results were observed when comparing interfacial friction factors, indicating that the majority of the effect of the polymer occurred at the gas-liquid interface.

While from all parameters it would appear that the maximum change occurred between 30 ppm and 40 ppm of DRA, a significant difference in the flow patterns and pressure drop was realized with addition of only 10 ppm DRA.

## BIBLIOGRAPHY

- Al-Sarkhi, A. and Hanratty, T. J. (2001a). Effect of drag-reducing polymers on annular gas-liquid flow in a horizontal pipe. *International Journal of Multiphase Flow*, 27:1151–1162.
- Al-Sarkhi, A. and Hanratty, T. J. (2001b). Effect of pipe diameter on the performance of drag-reducing polymers in annular gas-liquid flows. *Chemical Engineering Research and Design*, 79:402–408.
- Al-Sarkhi, A. and Soleimani, A. (2004). Effect of drag reducing polymers on two-phase gas-liquid flows in a horizontal pipe. *Chemical Engineering Research and Design*, 82:1583–1588.
- Baik, S. and Hanratty, T. J. (2003). Effects of a drag reducing polymer on stratified gas-liquid flow in a large diameter pipe. *International Journal of Multiphase Flow*, 29:1749–1757.
- Fernandes, R. J., Jutte, B. M., and Rodriguez, M. G. (2004). Drag reduction in horizontal annular two-phase flow. *International Journal of Multiphase Flow*, 30:1051–1069.

- Fore, R., Szwalek, J., and Sirviente, A. I. (2004). The effects of polymer solution preparation and injection on drag reduction. *Transactions of the ASME*, 127:536–549.
- Foshee, W. C., Jennings, R. R., and West, T. J. (1976). Preparation and test of partially hydrolyzed polyacrylamide solutions. *Society of Petroleum Engineers, 51st Annual Fall Technical Conference and Exhibition*, SPE 6202.
- Jovanovic, J., Pashtropanska, M., Frohnafel, B., Durst, F., Koskinen, J., and Koskinen, K. (2006). On the mechanism responsible for turbulent drag reduction by dilute addition of high polymers: theory, experiments, simulations and predictions. *Transactions of the ASME*, 128:118–130.
- Liberatore, M., Baik, S., McHugh, A., and Hanratty, T. J. (2004). Turbulent drag reduction of polyacrylamide solutions: effect of degradation on molecular weight distribution. *Journal of Non-Newtonian Fluid Mechanics*, 123:175–183.
- Little, R. C., Hansen, R. J., Huntson, D. L., Kim, O. K., Patterson, R. L., and Ting, R. Y. (1975). The drag reduction phenomenon. Observed characteristics, improved agents and proposed mechanisms. *Industrial and Engineering Chemical Fundamentals*, 14(4):283–286.
- Manfield, P. D., Lawrence, C. J., and Hewitt, G. F. (1999). Drag reduction

- with additives in multiphase flow: a literature survey. *Multiphase Science and Technology*, 11:197–221.
- Paras, S., Vlachos, N., and Karabelas, A. (1994). Liquid layer characteristics in stratified-atomization flow. *International Journal of Multiphase Flow*, 20(5):939–956.
- Sellin, R. H. J., Hoyt, J. W., and Scrivener, O. (1982). The effect of drag-reducing additives on fluid flows and their industrial applications. part I. Basic aspects. *Journal of Hydraulic Research*, 20(1):513–31.
- Sylvester, N. D. and Brill, J. P. (1976). Drag reduction in two-phase annular-mist flow of air and water. *AICHE Journal*, 22(3).
- Toms, B. A. (1948). Some observations on the flow of linear polymer solutions through straight tubes at larger Reynolds numbers. *Proceedings of the First International Congress on Rheology*, 2:135.
- Vlachogiannis, M., Liberatore, M. W., McHugh, A. J., and Hanratty, T. J. (2003). Effectiveness of a drag reducing polymer: relation to molecular weight distribution and structuring. *Physics of Fluids*, 15(12):3786–3794.
- Warholic, M. D., Massah, H., and Hanratty, T. J. (1999). Influence of drag reducing polymers on turbulence: effects of Reynolds number, concentration and mixing. *Experiments in Fluids*, 27:461–472.
- Zohourian-Mashmoul, M. J., Pourjavadi, A., and Nadali, M. (1994). Oil

soluble drag reducing polymers. *Journal of Polymer materials*, 11(4):239–247.

## CHAPTER 4

### CONCLUSION

Studies were done in order to acquire more information about the nature of the gas-liquid interface in horizontal stratified flow. Further studies were then undertaken in order to more fully understand the effect of a drag reducing polymer on the gas-liquid interface.

The apparatus was designed with a rectangular cross-section in order to focus on the interface of the flow. A non-contact film thickness measurement method using laser induced fluorescence and a video camera was then developed to visualize the interface. This measurement technique allowed for cross-stream measurements and measurements over time to be taken. The measurement method was designed to obtain a significant amount of information including interfacial waves, mean large amplitude wave heights, RMS wave heights and wave frequency.

Using this method, information was gathered about the wavy gas-liquid interface of the stratified flow. All the major characteristics of the gas-liquid

interface observed by other researchers in previous work were observed here as well.

Results, using the measurement technique, demonstrated that the addition of DRA to the flow caused suppression of the waves on the interface even with only an addition of 5 ppm. The shape of the wave was also altered with the addition of the polymer, such that conditions that would create large amplitude waves instead created waves that were more similar in appearance to 2-D waves.

The flow conditions and concentration of polymer that caused the maximum reduction in drag corresponded with the maximum reduction in mean large wave amplitude and with the maximum reduction in interfacial friction factor, signalling that the polymer had a large effect on the gas-liquid interface.

While the concentration of polymer that caused the greatest effect on the flow was between 30 ppm and 40 ppm, the difference in results between those concentrations and the results with the addition of 10 ppm was usually less than 10%. Thus while not producing the maximum drag reduction, the addition of 10 ppm DRA caused a very significant difference.

There are many adjustments to the set up and further experiments that could be conducted. There are a few specific adjustments that could be made to the apparatus and the experimental set-up. First the apparatus could be lengthened in order to ensure the fully developed flow assumption for two phase flow. In addition, the measurement system could be adjusted

to acquire information over the entire cross-section of the gas-liquid interface through the use of a larger cylindrical lens to enlarge the laser light sheet. In order to avoid further uncertainty a standard concentration of dye could also be used. To reduce some of the current uncertainty in the measurement system a more powerful laser and greater magnification of the camera lens could be used.

Further studies on the gas-liquid interface could also be done by using a stroboscope and photographing the interface in order to determine the effects of the wall on the shape of the waves. In addition the inlet conditions could be altered by changing the height of the floor thereby changing the height of the entering liquid stream.

Additional work could also be done in order to determine the effect of utilizing a master solution and injecting the DRA at different points along the fluid line rather than pumping in the solution thus exposing the DRA to shear stress and degradation. In addition further work into the rheological properties of the polymer is needed in order to more fully understand the effects it has on the flow.

## APPENDIX A

### ORIFICE PLATE

An orifice plate was used to calculate the air flow rate in the experiment. It was rectangular in cross section and had an inner cross-section of 20.3 mm by 40.6 mm and an outer cross-section the same as the duct cross-section. This corresponded to

$$\beta = \frac{d_t}{D} = 0.8 \quad (\text{A.1})$$

The taps were set at  $D_h$  upstream and  $1/2D_h$  downstream. The equation for the flow rate was given by the general relation for a Bernoulli obstruction meter.

$$Q = C_d A_t \left( \frac{2\Delta P/\rho}{1 - \beta^4} \right)^{1/2} \quad (\text{A.2})$$

In order to determine the flow rate for any given experiment, a discharge coefficient,  $C_d$  was required. An experiment was performed with an average

upstream pressure,  $P_{up}$ , of 95.5 kPa and an average differential pressure,  $P_{diff}$ , of 2.5 kPa across the orifice plate.

The air density was calculated by the ideal gas law:

$$\rho_G = \frac{P_{up}}{RT} \quad (\text{A.3})$$

These values were used in equation A.2. In order to determine  $C_d$  from that equation the following iterative process was used. First a velocity was assumed,  $U_{assume}$ . This value was then used to calculate the Reynolds number with the following equation:

$$Re = \frac{\rho U_{assume} D_h}{\mu} \quad (\text{A.4})$$

where the viscosity of air was taken at standard atmosphere and temperature.

The Reynolds number was then used to approximate the discharge coefficient using the curve fit formulas outlined by ISO 5167.

$$C_d = f(\beta) + 97.71\beta^{2.5}Re^{-0.75} + \frac{0.09\beta^4}{1 - \beta^4}F_1 - 0.0337\beta^3F_2 \quad (\text{A.5})$$

where:

$$f(\beta) = 0.5959 + 0.0312\beta^{2.1} - 0.184\beta^8 \quad (\text{A.6})$$

For pressure taps located at D upstream and 1/2D downstream the values for  $F_1$  and  $F_2$  are as follows:

$$F_1=0.4333 \text{ and } F_2=0.47$$

These values were used in equation A.2 to calculate the flow rate. From the flow rate the average velocity was calculated and compared with the assumed velocity. A program was designed to follow the iterative steps until  $U_{assume} = U_{calculated}$ .

Using this method a discharge coefficient of 0.6239 was calculated and was used for all the experiments performed. Based on verification of the orifice plate with a pitot tube, this assumption caused an error of 4%.

Using the discharge coefficient equation A.2 then became:

$$Q = 5.14 \times 10^{-6} \left( \frac{972.2TP_{diff}}{P_{up}} \right)^{1/2} \quad (A.7)$$

This equation was used to determine the air flow rate for each experiment.

## APPENDIX B

### DIGITAL FILTER

A digital filter was used to remove the high frequency noise in the wavy film thickness measurements. The data was filtered forward and in the reverse direction in order to ensure a zero-phase distortion.

An Equiripple filter was used with a sampling frequency of 1000 Hz, a passband frequency of 100 Hz and a stopband frequency of 150 Hz. The passband weight was 400 and stopband weight was 10. The filter had an order of 20 and a density factor of 20 as well. Figure B.1 shows the magnitude response of the filter.

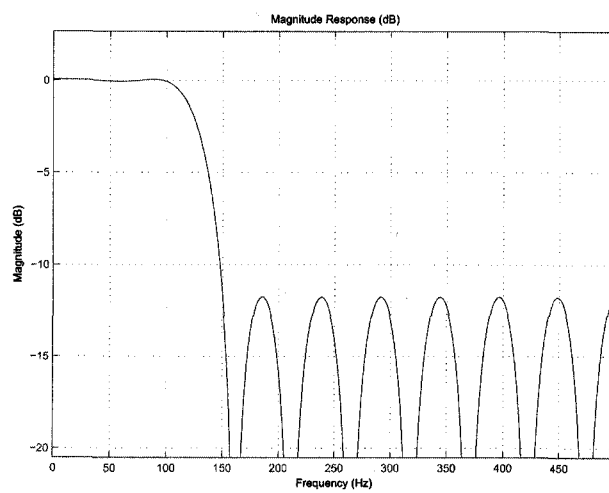


Figure B.1: Magnitude response of the digital Equiripple filter